

Ballistic-hydrodynamic phase transition in Poiseuille flow of two-dimensional electrons

A. N. Afanasiev, P. S. Alekseev, A. A. Greshnov, and M. A. Semina
Ioffe Institute, Politekhmicheskaya 26, 194021 St. Petersburg, Russia

Phase transitions are characterized by a pronounced change in the type of dynamics of microparticles or of the ordering. A description of phase transitions usually requires quantum statistics. Recently, a peculiar type of conductors was discovered in which two-dimensional (2D) electrons form a viscous fluid. Here we report a novel type of phase transitions in such systems between the ballistic and the hydrodynamic states of classical 2D electrons in external magnetic fields. We trace an abrupt emergence of a fluid phase of interacting hydrodynamic electrons from a “dust” of ballistic electrons with an increase of magnetic field. This transition manifests itself in a kink in the dependence of the longitudinal and the Hall resistances on magnetic field, reflecting the switching of the type of the particle dynamics below and above the critical magnetic field. Apparently, such transition was observed in the recent experiments on 2D electron hydrodynamics in graphene and high-mobility GaAs quantum wells. The obtained results reveal the mechanism of a formation of a thermodynamic fluid phase from individual ballistic particles in high-quality samples.

1. Introduction. Frequent collisions between electrons in high-quality conductors at low temperatures can lead to formation of a viscous electron fluid and the realization of the hydrodynamic regime of charge transport. Although the theory of such fluid has been actively developed for a very long time [20],[21] the formation of the viscous flow of an electron fluid was unambiguously demonstrated only recently in experiments on high-quality graphene, Weyl semimetals, and GaAs quantum wells [1]-[19]. The hydrodynamic flow in these experiments was detected by a specific dependence of the mean sample resistivity on the sample width [1]; by observation of the negative nonlocal resistance [2, 3, 13], the giant negative magnetoresistance [7–12, 14, 15], and the huge magnetic resonance at twice cyclotron frequency [16–19].

Much attention was paid to the description of the transition between the ballistic and the hydrodynamic regimes of electron transport. In Ref. [6] analysis of the measured profiles of the Hall field in a Poiseuille flow in a graphene stripe made it possible to study the transition between the ballistic and the hydrodynamic regimes occurring with changing of magnetic field and temperature. As for theoretical works, in Ref. [22] this transition was considered for 2D electrons in a sample with randomly located localized obstacles in the absence of magnetic field. It was shown that the transition to the hydrodynamic regime is smooth, displaying the nature of a crossover.

In a perpendicularly applied magnetic field, the ballistic-hydrodynamic transition was numerically studied for a Poiseuille flow of two-dimensional electrons in a long sample in Ref. [23]. It was shown that for a magnetic field at which the diameter of the electron cyclotron orbit $2R_c$ coincides with the sample width W , $W = 2R_c$, the longitudinal and the Hall resistances as functions of the magnetic field exhibit a kink. In Ref. [24], a flow of 2D electrons in a stripe in the presence of a magnetic field was studied in more details. In particular, the profiles of the Hall electric field over the sample cross section were calculated and an analytical solution of the kinetic

equation was constructed in the ballistic regime. The transition between the ballistic and the hydrodynamic regimes was studied by the numerical solution of the kinetic equation numerically. It is at the transition the sharpening of the Hall field profile together and a large increase of its curvature take place. In Refs. [25, 26], the flow of interacting electrons in a narrow ballistic sample in a very weak magnetic field was analytically studied. It was shown that inter-particle collisions lead to small corrections to the magnetoconductance and the Hall electric field, being the precursors of formation of the viscous flow.

In this work, we reveal the phase transition between the ballistic and the hydrodynamic phases of two-dimensional electrons in narrow ultra-high-mobility samples in a magnetic field. We demonstrate that the electron dynamics qualitatively changes when the magnetic field B crosses the critical field B_c corresponding to $2R_c = W$, although it is controlled by the electron-electron scattering in the whole vicinity of the phase transition ($2R_c \approx W$), even in the ballistic regime ($2R_c > W$). This phase transition is closely related to the possibility to make a complete cyclotron loop without edge scattering when B becomes greater than B_c that corresponds to $2R_c < W$. Using the developed mean-field-like model we analytically calculate the longitudinal and the Hall resistances ρ_{xx} and ρ_{xy} as functions of the magnetic field and show that they have a kink at the transition point $B = B_c$. In the whole range of the magnetic fields, below and above B_c , the functions $\rho_{xx}(B)$ and $\rho_{xy}(B)$ exhibit a nontrivial non-monotonous behavior, being in a good agreement with numerical theory [23, 24] and experimental results [6, 14].

In the ballistic phase when $B < B_c$, 2D electrons also show quite non-trivial behavior, including the ballistic magnetoresistance anomaly in the Hall resistance $\rho_{xy}(B)$ [27]. In this work, we provide a simple and transparent derivation of the remarkable fact that the Hall resistance of narrow ballistic samples at very low magnetic fields is

equal to one half of the conventional Hall resistance of Ohmic samples: $\varrho_{xy} = \varrho_{xy}^{(0)}/2 = B/(2nec)$ [26]. Using the solution of the kinetic equation for electrons in such samples, similar to the one constructed in Ref. [24], we also show that the Hall field profile near the edges of the sample has non-analytical features and is divergent.

2. *Model.* We consider a flow of two-dimensional electrons in a long sample with rough edges. Electrons are supposed to be scattered at the edge diffusively, so that reflected electrons completely lose their pre-collision momenta. In the bulk of the sample, electrons collide with each other and/or are scattered by the bulk disorder (see Fig. 1). Our approach allows one to consider the systems being the mixtures of the two extreme cases: (i) there are no bulk defects and the electrons inside the sample are scattered only on each other, conserving momentum; or (ii) there are no inter-particle collisions, but inside the sample the scattering of electrons by a weak disorder, leading to a weak momentum relaxation, takes place. We assume that the rate γ of any bulk scattering is weak, $W \ll l$ (here $l = v_F/\gamma$ is the electron mean free path and v_F is the characteristic velocity of electrons).

At low magnetic fields $B < B_c$ when the diameter of the cyclotron circle is larger than the sample width, $2R_c > W$, each electron is predominantly scattered on the sample edges [see Figs. 1(a,b); $R_c = v_F/\omega_c$ is the cyclotron radius and $\omega_c = eB/(mc)$ is the cyclotron frequency]. Therefore the transport regime at such B is ballistic, and the interparticle collisions can only limit the time which the electrons spend on the ballistic trajectories.

At high magnetic fields, $B > B_c$, corresponding to $W > 2R_c$, electrons are divided into two groups: the edge electrons that move predominantly along the skipping orbits intersecting only one of the two longitudinal edges, and the central electrons whose trajectories do not touch the edges [see Figs. 1(c)]. The central electrons collide mainly with the edge electrons (and/or scatter on bulk disorder) anticipating the formation of the bulk electrons phase, responsible for the hydrodynamic/Ohmic transport in wide samples, $W \gg R_c$.

3. *The ballistic regime.* In the ballistic regime the electron dynamics does not exhibit collective effects far from the transition and is described, in the main order by the bulk scattering rate, by the kinetic equation with the omitted arrival term in the collision integral [24, 29]. The solution of such equation [29] shows that the ballistic regime has a fine structure, namely, it is divided into three subregimes. The transition between them is accompanied by the evolution of the current density $j(y)$ and the Hall electric field $E_H(y)$ [see Fig. 2(a)-(c)] as well as by a nonmonotonic behavior of the longitudinal $\varrho_{xx}(B)$ and the Hall resistances $\varrho_{xy}(B)$ [see Fig. 3], those are known as the “ballistic magnetoresistance anomalies” [27].

In the first ballistic subregime, $R_c \gg l^2/W$, the elec-

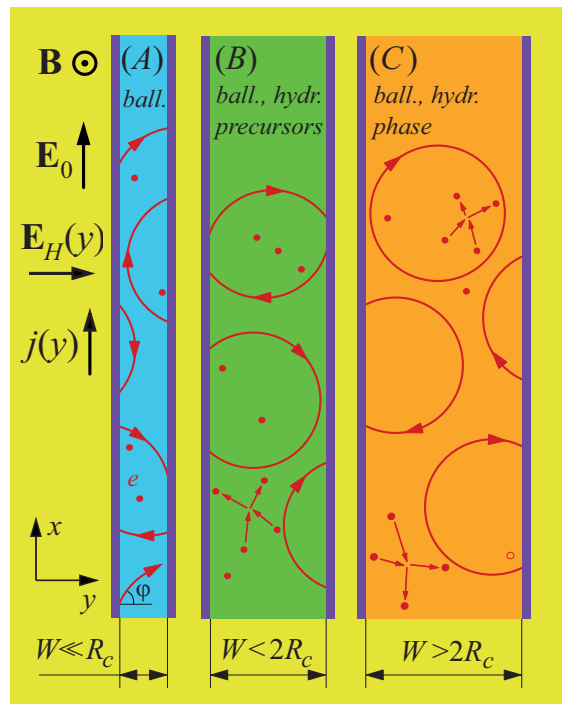


FIG. 1: Two-dimensional electrons in a long sample at low, $W \ll R_c$, (a); intermediate, $W \sim R_c$, $W < 2R_c$, (b); and moderately high, $W \sim R_c$, $W > 2R_c$, (c) magnetic fields. At the critical field B_c corresponding to the condition $2R_c = W$ the ballistic-hydrodynamic phase transition occurs. Above it, $B > B_c$, a group of central electrons appears that do not collide with the edges. In the low vicinity of the transition point, $0 < B_c - B \ll B$, electrons mainly populate the skipping orbits consisting of almost whole cyclotron rotations.

tron trajectories are almost straight and corrections from the electric and the magnetic fields are small. The magnitude of the current density, j , is controlled by the mean free path, calculated by averaging of the lengths $l_b(\varphi)^{(1)} = W/\cos\varphi$ of the ballistic trajectories over the angle φ between the electron velocity and the normal to the edges [see Fig. 1(a)]. The trajectories being almost parallel to the sample edge, $|\varphi| \approx \pi/2$, provide the main contribution to the current [25]. Their maximum length is limited by the shortest of the sample length and the mean free path due to interparticle scattering (or scattering on bulk defects). Calculation leads to the result $j = (2j_0/\pi) \ln[1/(\gamma W)]$, where $j_0 = nE_0W/m$ and the logarithm originates from the integration of the contribution to j from the interval $(\varphi, \varphi + d\varphi)$ over the angles $|\pi/2 - |\varphi|| \lesssim W/l$.

The magnetic Lorentz force induces a small disturbance on the ballistic trajectories in this subregime. Correspondingly, the longitudinal resistance $\varrho_{xx}(B)$ decrease with magnetic field [see Fig. 3(a)] due to the increase of the average length $l_b^{(1)}$ of the trajectories caused by their bending by the magnetic Lorentz force [25, 29]. The Hall resistance turns out to be one half of the con-

ventional Hall resistance of macroscopic samples in the Ohmic regime at zero temperatures [26]:

$$\varrho_{xy} = \frac{1}{2} R_H^0 B, \quad R_H^0 = \frac{1}{nec}, \quad (1)$$

In Ref. [26] this surprising result was obtained as a result of solution of the kinetic equation. In this work we succeeded in revealing of the origin of this remarkable behavior of ϱ_{xy} .

Indeed, in this limit of weak magnetic fields, $\omega_c \ll \gamma^2 W$ the motion of electrons along the axis x is governed mainly by the electric field E and is described by the formula $v_x(t) = v_F \sin \varphi + Et/m$, where the time t is counted from the last scattering at an edge. Correspondingly, the magnetic Lorentz force linearly depends on time t as $F_y^L(t) = eBv_x(t)/c$. The Hall electric field E_H , which compensates this force, is calculated by averaging over all electrons with any y and φ , using the dependence $t = t(y, \varphi)$ for unperturbed trajectories. As a result, the field E_H acquires the factor 1/2 from averaging of the linear in t term in F_y^L . This straightforward simple calculations [29] leads to result (1).

We conclude that at $B, T \rightarrow 0$ the ballistic Hall resistance (1), similarly to the Hall resistance $\varrho_{xy} = R_H^0 B$ in the Ohmic and the hydrodynamic regimes, indicates purely mechanical and thermodynamical (not kinetic) properties of the system. It is noteworthy that a similar result concerning the thermodynamical nature of ϱ_{xy} at $B \rightarrow 0$ for any conductor at very low temperatures was recently formulated and proved in in Ref. [28].

In the second ballistic subregime, $W \ll R_c \ll l^2/W$, electron paths become more and more bent [see Fig. 1(b)]. Their maximal length is now limited by geometry and is estimated as the size of the largest segment of a cyclotron circle that can be inscribed in the sample. Interparticle collisions lead only to small corrections to all observable quantities. The corresponding estimate for the longest electron trajectories is: $l_b^{(2)} \sim \sqrt{R_c W}$. Since the initial and the final angles of the electron velocity on such trajectories satisfy the condition $\pi/2 - |\varphi| \sim W/l_b^{(2)}$, the current is given by the formula similar to the one of the first ballistic subregime, but with different argument of the logarithm: $j = (2j_0/\pi) \ln(1/\sqrt{\omega_c W})$ [29] [see Fig. 3(a)]. Herewith, due to a nontrivial properties of such curved trajectories at different φ , the Hall electric field turns out to be independent of B , $E_H(B) = \text{const}$ [29]. So the Hall resistance $\varrho_{xy}(B) = E_H/j$ acquires a non-trivial singular behavior in this ballistic subregime [see Fig. 3(b)], previously obtained in numerical simulation of the ballistic transport and named the ballistic magnetoresistance anomaly [27].

In the third ballistic subregion, $\gamma W^2 \ll 2R_c - W \lesssim W$, a large part of non-equilibrium electrons, after scattering on a sample edge, returns to the same edge. Herewith an imbalance in the number of the electrons on such skipping trajectories intersecting only the left or only the right

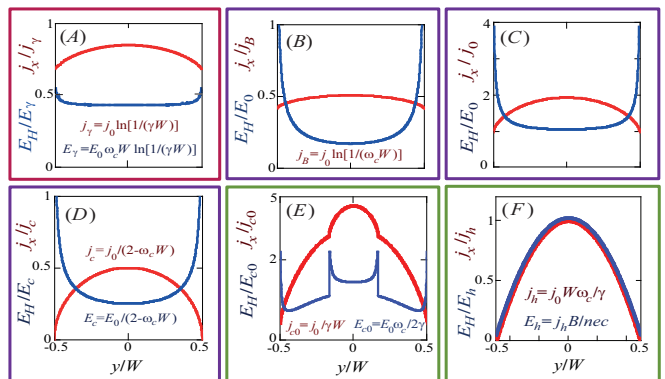


FIG. 2: Current density $j(y)$ and Hall electric field $E_H(y)$ at various magnetic fields B lying in: (a) the first ballistic subregime, $R_c \gg l^2/W$; (b) the second ballistic subregime, $W \ll R_c \ll l^2/W$; (c) the third ballistic subregime, $W < 2R_c \lesssim W$ (namely, $R_c = W$); (d) the very point of the ballistic-hydrodynamic phase transition, $W = 2R_c$; (e) the field far above the transition point, $W = 3R_c$ (schematically); and (f) a well-formed Poiseuille flow, $W \gg R_c$ (schematically).

edges appears [29]. Some of such left-edge and right-edge electrons undergo an almost complete turn over the cyclotron circle [see Fig. 1(b)], that leads to more regular character of their motion and to suppressed momentum relaxation. The last is mainly determined by the rare scattering on the opposite edge. In this way, the main contribution to j and E_H originates from such electrons on the skipping orbits, and the magnitudes of the current density j and the Hall field E_H significantly increase as compared with the lower fields, when $R_c \sim W$.

The distributions of the current density $j(y)$ and the Hall field $E_H(y)$ in the first ballistic subregime, $\omega_c \ll \gamma^2 W$, are almost flat, except for the small sharp features near the edges with infinitely large curvature at $y \rightarrow \pm W/2$ [see Fig. 2(a)]. These singularities are associated with the electrons on the trajectories colliding with the edges at very small angles, $|\pi/2 - |\varphi|| \ll 1$. Indeed, such electrons spend much longer time in the vicinity of the edges as compared to the electrons with $|\pi/2 - |\varphi|| \sim 1$. In the second and the third ballistic subregimes, the profiles $j(y)$ and $E_H(y)$ become more curved due to the increase of the number of the electrons touching the edges [see Fig. 2(b,c)]. The similar profiles for the second and third ballistic subregimes were obtained in Ref. [24].

4. The phase transition. Next, we show that in the vicinity of the critical $B = B_c$, where $W = 2R_c$, a phase transition occurs between a “heap” of almost independent ballistic electrons and a thermodynamic system of interacting electrons. The last one is the nucleus of the thermodynamic phase of the electron fluid realizing the hydrodynamic or the Ohmic transport.

Just below the transition, when $2R_c > W$ and the parameter $2 - W/(2R_c)$ approaches to $\gamma W \ll 1$, the im-

balance in the numbers of the left-edge and the right-edge electrons on the skipping orbits increases dramatically [29]. The balance of electron densities and their contributions to the current is controlled by comparable contributions from rare collisions of the skipping electrons with the opposite edges and from collisions of skipping electrons with each other. The interparticle scattering of the skipping electrons becomes more and more important for the relaxation of the electron momentum with approaching of the parameter W/R_c to two [29]. Consequently, the values j and E_H at $2R_c \rightarrow W$ become proportional to the scattering time $1/\gamma$.

Above the transition point, at $W > 2R_c$, the central electrons protected from the scattering on the edges emerge [see Fig. 1 (c)]. Their relative density $\alpha_c = n_c/n$ depends on magnetic field as $\alpha_c = (W - 2R_c)/W$. When $\alpha_c \ll 1$, than the relative density of the edge electrons is close to unity, $\alpha_e \equiv n_e/n = 1 - \alpha_c$, and the center electrons lose their momenta predominantly via scattering on electrons at the edge skipping orbits. They provide a contribution to the current and the Hall field being different from the one from the edge electrons.

Such a change in the electron dynamics above and below the transition, accompanied by a kink in the curves $\varrho_{xx}(B)$ and $\varrho_{xy}(B)$ (see Fig. 3), indicates that the forming of the hydrodynamic transport regime from the ballistic one is a phase transition. The relative density of the central electrons, α_c , can be chosen as the order parameter of this transition. In the lower vicinity of the transition point, $0 < B_c - B \ll B_c$, the described above electrons on the skipping orbits with the momentum relaxation time going to $\sim 1/\gamma$ at $2R_c \rightarrow W$ is a precursor of the hydrodynamic phase of the central electrons, appearing at $B > B_c$.

With the increase of magnetic field, the relative density of the central electrons increases and their collisions with each other become important. At $\alpha_c \sim 1$, the current density of central electrons becomes y -dependent as the closer is a center electron to the sample center, $y = 0$, the less important is its scattering on the edge electrons and more important on other center electrons. This is the beginning of the formation of the viscous Poiseuille flow [see Fig. 2(e)]. When the cyclotron radius becomes very small, $R_c \ll W$, the central electrons dominate everywhere except the vicinities of the edges, $W/2 - |y| \sim R_c$ [see Fig. 2(f)]. The longitudinal resistance ϱ_{xx} is now determined by viscosity, $\varrho_{xx} \sim \eta_{xx}$, where $\eta_{xx} \sim \gamma/\omega_c^2$, while the Hall resistance ϱ_{xy} turns out to be close to the universal constant $\varrho_{xy}^0 = B/(ne^c)$ [15].

A similar phase transition with the increase of magnetic field occurs between the ballistic and the Ohmic regimes, when electrons are scattered on bulk disorder, and there is no interparticle scattering [29]. The character of the electron dynamics below the transition, $B < B_c$, and the dynamics of the edge electrons

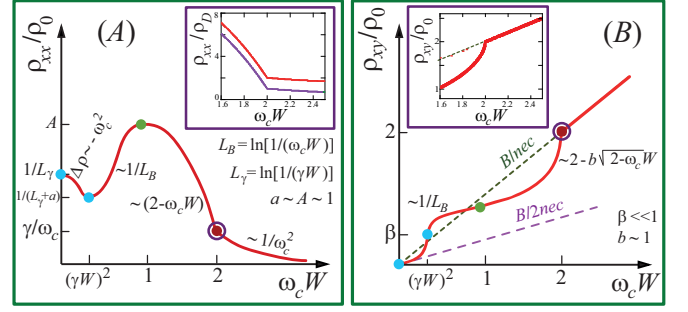


FIG. 3: Longitudinal ϱ_{xx} (a) and Hall ϱ_{xy} (b) resistances as functions of magnetic field normalized on the constant $\varrho_0 = mW/(ne^2)$. For the first ($R_c \gg l^2/W$), the second ($W \ll R_c \ll l^2/W$) and the right part of the third ($0 < 2 - W/R_c \ll 1$) ballistic subregimes, as well as for the well-formed Poiseuille flow ($W \gg R_c$) the asymptotic behaviors of the dependencies $\varrho_{xx}(\omega_c)$ and $\varrho_{xy}(\omega_c)$ are depicted near the corresponding parts of the curves. Insets show the behavior of $\varrho_{xx}(\omega_c)$ and $\varrho_{xy}(\omega_c)$ near the transition point $\omega_c W = 2$.

above the transition, $B > B_c$ are very similar to ones in the ballistic-hydrodynamic transition in the pure system, while the central electrons at $B > B_c$ are now a precursor of the bulk Ohmic phase, in which electrons are scattered only on the bulk disorder.

Quantitatively, we describe the ballistic-hydrodynamic and the ballistic-Ohmic phase transitions by a simple mean-field-like model taking into account the diffusive scattering of electrons on the sample edges and weak inter-particle collisions conserving both momentum and number of particles (or weak scattering on disorder) [29]. The key simplification of our model is using the collision integral with the arrival term averaged over the sample cross section. Such kinetic equation preserves momentum and/or the number of particles in collisions only in the whole sample, but not at each point y .

The current density distributions, calculated within our model in the lower vicinity of the transition point, $2 - W/R_c \sim \gamma W$ have the form of a semicircle [see Fig. 2(d)]:

$$j(y) = j_c \sqrt{1 - (y/R_c)^2}. \quad (2)$$

Here $j_c = 4ne^2 E_0 / [\pi m(\gamma + 2\varepsilon)]$ and $\varepsilon = (2 - W/R_c)v_F / (\pi R_c) \ll v_F/R_c$ is the parameter characterizing the proximity to the transition point. At $\varepsilon \rightarrow 0$ the current amplitude diverges, and its maximum value is limited by the scattering rate. Current density (2) originates from the excess and the lack of electrons at the skipping orbits on the left and the right sample edges. The corresponding Hall electric field takes the form:

$$E_H(y) = \frac{E_c}{\sqrt{1 - (y/R_c)^2}}, \quad (3)$$

where $E_c = 2E_0 \omega_c / [\pi(\gamma + 2\varepsilon)]$.

For magnetic fields far above the transition, $W > 2R_c$, $W - 2R_c \sim R_c$, when a large number of the central electrons appears, $\alpha_c \sim 1$, the current density $j(y)$ and the Hall field $E_H(y)$ profiles are schematically shown on Fig. 2(e). Such profiles take into account the contribution from the central electrons with smooth profiles of $j(y)$ and $E_H(y)$ as well as the contributions from the edge electrons with the profiles $j(y)$ and $E_H(y)$ similar to Eqs. (2) and (3) with the properly shifted centers $y = \pm(W/2 - R_c)$. Thus, the current and the field profiles $j(y)$ and $E_H(y)$ have singularities at $y = \pm W/2$ and $y = \pm(W/2 - 2R_c)$ [compare Figs. 2(a-d) and 2(e)]. In a well-formed Poiseuille hydrodynamic flow, both functions $j(y)$ and $E_H(y)$ are parabolic, excepting for the narrow near-edge regions [see Fig. 2(f)].

Transformation of dynamics of the the edge electrons with crossing the critical point $B = B_c$ and the emergence of the central electrons at $B > B_c$ lead to a non-analytical behavior of all macroscopic quantities. In particular, a kink in the dependence of the longitudinal ϱ_{xx} and the Hall ϱ_{xy} averaged resistances on magnetic field appears at $B = B_c$. Calculation in the framework of the developed model [29] yields for the vicinity of the ballistic-hydrodynamic phase transition, $|W - 2R_c| \ll W$ (see also Fig. 3):

$$\varrho_{xx}(B) = \frac{m}{ne^2} \begin{cases} \gamma + 2\varepsilon, & B < B_c \\ \gamma(1 - 2\alpha_c), & B > B_c \end{cases} \quad (4)$$

and

$$\varrho_{xy}(B) = \frac{B}{nec} \begin{cases} 1 - \sqrt{2\varepsilon/\pi}, & B < B_c \\ 1, & B > B_c \end{cases} \quad (5)$$

For the ballistic-Ohmic phase transition the resulting dependencies $\varrho_{xx}(B)$ and $\varrho_{xy}(B)$ are similar to Eqs. (4) and (5), but have other numeric coefficients [29]. It is noteworthy that the Hall constant $R_H = \varrho_{xy}/B$ right above the transition becomes R_H^0 (at least, in the main order by γ), that coincides with the one in the Ohmic regime at low temperatures (see discussion in [29]).

In Supplementary Materials [29], we compare our results with preceding theoretical [23, 24] and experimental [6, 14] works. We discuss that in Refs. [6, 14] the ballistic-hydrodynamic transition was observed. In particular, the experimental dependencies $\varrho_{xx}(B)$ and $\varrho_{xy}(B)$ are quite similar to the ones shown in Fig. 3.

5. Conclusion and Acknowledgements. A novel type of phase transitions is revealed and studied, which, we believe, can be realized in a wide class of systems. A good candidate for this is high-quality GaAs quantum wells with rare macroscopic defects studied, for example, in Ref. [30]. Analysis of Refs. [15],[25] shows that, apparently, 2D electrons in them are scattered predominantly on the defects at weak magnetic field, while at sufficiently strong field, when the cyclotron diameter $2R_c$ becomes smaller than the typical distances between the defects,

the electron-electron scattering leads to formation of a viscous electron fluid in a space between the defects.

We thank A. I. Chugunov and A. V. Shumilin for fruitful discussions. The study was supported by the Russian Fund for Basic Research (Grant No. 19-02-00999) and by the Foundation for the Advancement of Theoretical Physics and Mathematics "BASIS".

-
- [1] P. J. W. Moll, P. Kushwaha, N. Nandi, B. Schmidt, and A. P. Mackenzie, Evidence for hydrodynamic electron flow in PdCoO₂, *Science* **351**, 1061 (2016).
 - [2] D. A. Bandurin, I. Torre, R. Krishna Kumar, M. Ben Shalom, A. Tomadin, A. Principi, G. H. Auton, E. Khestanova, K. S. Novoselov, I. V. Grigorieva, L. A. Ponomarenko, A. K. Geim, and M. Polini, Negative local resistance caused by viscous electron backflow in graphene, *Science* **351**, 1055 (2016).
 - [3] L. Levitov and G. Falkovich, Electron viscosity, current vortices and negative nonlocal resistance in graphene, *Nature Physics* **12**, 672 (2016).
 - [4] R. Krishna Kumar, D. A. Bandurin, F. M. D. Pellegrino, Y. Cao, A. Principi, H. Guo, G. H. Auton, M. Ben Shalom, L. A. Ponomarenko, G. Falkovich, K. Watanabe, T. Taniguchi, I. V. Grigorieva, L. S. Levitov, M. Polini, and A. K. Geim, Superballistic flow of viscous electron fluid through graphene constrictions, *Nature Physics* **13**, 1182 (2017).
 - [5] A. I. Berdyugin, S. G. Xu, F. M. D. Pellegrino, R. Krishna Kumar, A. Principi, I. Torre, M. Ben Shalom, T. Taniguchi, K. Watanabe, I. V. Grigorieva, M. Polini, A. K. Geim, and D. A. Bandurin, Measuring Hall viscosity of graphene's electron fluid, *Science* **364**, 162 (2019).
 - [6] J. A. Sulpizio, L. Ella, A. Rozen, J. Birkbeck, D. J. Perello, D. Dutta, M. Ben-Shalom, T. Taniguchi, K. Watanabe, T. Holder, R. Queiroz, A. Principi, A. Stern, T. Scaffidi, A. K. Geim, and S. Ilani, Visualizing Poiseuille flow of hydrodynamic electrons, *Nature* **576**, 75 (2019).
 - [7] J. Gooth, F. Menges, C. Shekhar, V. Suess, N. Kumar, Y. Sun, U. Drechsler, R. Zierold, C. Felser, and B. Gotsmann, Thermal and electrical signatures of a hydrodynamic electron fluid in tungsten diphosphide, *Nature Communications* **9**, 4093 (2018).
 - [8] L. Bockhorn, P. Barthold, D. Schuh, W. Wegscheider, and R. J. Haug, Magnetoresistance in a high-mobility two-dimensional electron gas, *Phys. Rev. B* **83**, 113301 (2011).
 - [9] A. T. Hatke, M. A. Zudov, J. L. Reno, L. N. Pfeiffer, and K.W. West, Giant negative magnetoresistance in high-mobility two-dimensional electron systems, *Phys. Rev. B* **85**, 081304 (2012).
 - [10] R. G. Mani, A. Kriisa, and W. Wegscheider, Size-dependent giant-magnetoresistance in millimeter scale GaAs/AlGaAs 2D electron devices, *Scientific Reports* **3**, 2747 (2013).
 - [11] Q. Shi, P. D. Martin, Q. A. Ebner, M. A. Zudov, L. N. Pfeiffer, and K. W. West, Colossal negative magnetoresistance in a two-dimensional electron gas, *Phys. Rev. B* **89**, 201301 (2014).

- [12] G. M. Gusev, A. D. Levin, E. V. Levinson, and A. K. Bakarov, Viscous electron flow in mesoscopic two-dimensional electron gas, *AIP Advances* **8**, 025318 (2018).
- [13] A. D. Levin, G. M. Gusev, E. V. Levinson, Z. D. Kvon, and A. K. Bakarov, Vorticity-induced negative nonlocal resistance in a viscous two-dimensional electron system, *Phys. Rev. B* **97**, 245308 (2018).
- [14] G. M. Gusev, A. D. Levin, E. V. Levinson, and A. K. Bakarov, Viscous transport and Hall viscosity in a two-dimensional electron system, *Phys. Rev. B* **98**, 161303 (2018).
- [15] P. S. Alekseev, Negative Magnetoresistance in Viscous Flow of Two-Dimensional Electrons, *Phys. Rev. Lett.* **117**, 166601 (2016).
- [16] Y. Dai, R. R. Du, L. N. Pfeiffer, and K. W. West, Observation of a Cyclotron Harmonic Spike in Microwave-Induced Resistances in Ultraclean GaAs/AlGaAs Quantum Wells, *Phys. Rev. Lett.* **105**, 246802 (2010).
- [17] A. T. Hatke, M. A. Zudov, L. N. Pfeiffer, and K. W. West, Giant microwave photoresistivity in high-mobility quantum Hall systems, *Phys. Rev. B* **83**, 121301 (2011).
- [18] M. Bialek, J. Lusakowski, M. Czapkiewicz, J. Wrobel, and V. Umansky, Photoresponse of a two-dimensional electron gas at the second harmonic of the cyclotron resonance, *Phys. Rev. B* **91**, 045437 (2015).
- [19] P. S. Alekseev and A. P. Alekseeva, ransverse Magnetosonic Waves and Viscoelastic Resonance in a Two-Dimensional Highly Viscous Electron Fluid, *Phys. Rev. Lett.* **123**, 236801 (2019).
- [20] R. N. Gurzhi, Hydrodynamic effects in solids at low temperatures, *Sov. Phys. Uspekhi* **94**, 657 (1968).
- [21] M. Hruska and B. Spivak, Conductivity of the classical two-dimensional electron gas, *Phys. Rev. B* **65**, 033315 (2002).
- [22] H. Guo, E. Ilseven, G. Falkovich, and L. Levitov, Higher-than-ballistic conduction of viscous electron flows, *PNAS* **114**, 3068 (2017).
- [23] T. Scaffidi, N. Nandi, B. Schmidt, A. P. Mackenzie, and J. E. Moore, Hydrodynamic Electron Flow and Hall Viscosity, *Phys. Rev. Lett.* **118**, 226601 (2017).
- [24] T. Holder, R. Queiroz, T. Scaffidi, N. Silberstein, A. Rozen, J. A. Sulpizio, L. Ella, S. Ilani, and A. Stern, Ballistic and hydrodynamic magnetotransport in narrow channels, *Phys. Rev. B* **100**, 245305 (2019).
- [25] P. S. Alekseev and M. A. Semina, Ballistic flow of two-dimensional interacting electrons, *Phys. Rev. B* **98**, 165412 (2018).
- [26] P. S. Alekseev and M. A. Semina, Hall effect in a ballistic flow of two-dimensional interacting particles, *Phys. Rev. B* **100**, 125419 (2019).
- [27] C. W. J. Beenakker and H. van Houten, Quantum Transport in Semiconductor Nanostructures, *Solid State Physics* **44**, 1 (1991).
- [28] A. Auerbach, Hall Number of Strongly Correlated Metals, *Phys. Rev. Lett.* **121**, 066601 (2018).
- [29] For the details of the model and of the calculations as well as for the detailed comparison with preceding works see Supplementary Materials below.
- [30] L. Bockhorn, I. V. Gornyi, D. Schuh, C. Reichl, W. Wegscheider, and R. J. Haug, Magnetoresistance induced by rare strong scatterers in a high-mobility two-dimensional electron gas *Phys. Rev. B* **90**, 165434 (2014).

Supplementary Materials

1. MODEL

In order to study the transitions of 2D electron transport from the ballistic regime to the hydrodynamic or the Ohmic regimes, we consider a flat flow in a long sample with the width W and the length $L \gg W$. Herewith we use the simplified forms of the electron-electron and the disorder collision integrals, allowing the analytical solution of the kinetic equation. Such model has been used in Refs. [25, 26] to study the ballistic transport of 2D interacting electrons (here and below citations [1], [2], and so on refer to the bibliography of the main text).

We seek for the linear response to a homogeneous electric field $\mathbf{E}_0 \parallel x$ in the presence of external magnetic field \mathbf{B} perpendicular to the sample plane (see Fig. 1 in the main text). The corresponding distribution function of 2D electrons acquires the nonequilibrium part:

$$\delta f(y, \mathbf{p}) = -f'_F(\varepsilon) f(y, \varphi, \varepsilon) \sim E_0, \quad (\text{S1})$$

where $f_F(\varepsilon)$ is the Fermi distribution function, ε is the electron energy, φ is the angle of the electron velocity $\mathbf{v} = v(\varepsilon)[\sin \varphi, \cos \varphi]$ and the normal to the left sample edge, $\mathbf{p} = m\mathbf{v}$ is the electron momentum, and m is the electron mass. The dependence of δf on the coordinate x is absent since $L \gg W$. We also omit the energy dependence of the electron velocity $v(\varepsilon) = |\mathbf{v}(\varepsilon)|$ and the nonequilibrium part of distribution function $\delta f(y, \mathbf{p})$. Such simplification is valid for degenerate degenerate distribution. Hereinafter, we use the units of all values in which the characteristic electron velocity $v(\varepsilon) \equiv v_F$ and the electron charge e are set to be unity. Therefore, coordinate, time, and reciprocal electric field, $1/E_0$, have the same units.

The kinetic equation for the inequilibrium distribution function $f(y, \varphi)$ takes the form:

$$\cos \varphi \frac{\partial f}{\partial y} - \sin \varphi E_0 - \cos \varphi E_H - \omega_c \frac{\partial f}{\partial \varphi} = \text{St}[f], \quad (\text{S2})$$

where $\omega_c = eB/mc$ is the cyclotron frequency, E_H is the Hall electric field arising due to redistribution of particles in the presence of magnetic field, and the collision integral $\text{St}[f]$ describes both momentum-conserving electron-electron collisions and dissipative scattering by the bulk disorder. We use the following simplified form of $\text{St}[f]$:

$$\text{St}[f] = -\gamma f + \gamma_{ee} \hat{P}[f] + \gamma_d \hat{P}_0[f], \quad (\text{S3})$$

where γ_{ee} and γ_d are electron-electron and disorder scattering rates, $\gamma = \gamma_{ee} + \gamma_d$ is the total scattering rate, \hat{P} and \hat{P}_0 are the projector operators of the functions $f(\varphi)$ onto the subspaces $\{1, e^{\pm i\varphi}\}$ and $\{1\}$, respectively. Such collision integral conserves perturbations of the distribution function corresponding to a nonequilibrium density.

It also describes the conservation of momentum in the processes of inter-particle collisions.

We consider that the longitudinal sample edges are rough. Thus the scattering of electrons on the edges is diffusive and the boundary conditions for the distribution function have the form: [27],[26] (see Fig. 1 in the main text)

$$\begin{aligned} f(-W/2, \varphi) &= c_l, \quad -\pi/2 < \varphi < \pi/2, \\ f(W/2, \varphi) &= c_r, \quad \pi/2 < \varphi < 3\pi/2, \end{aligned} \quad (\text{S4})$$

where the quantities $c_l = c_l[f]$ and $c_r = c_r[f]$ are proportional to the y components of the incident particle flow on the left ($y = -W/2$) and the right ($y = W/2$) sample edges:

$$c_l = -\frac{1}{2} \int_{\pi/2}^{3\pi/2} d\varphi' \cos \varphi' f(-W/2, \varphi'), \quad (\text{S5})$$

$$c_r = \frac{1}{2} \int_{-\pi/2}^{\pi/2} d\varphi' \cos \varphi' f(W/2, \varphi').$$

These boundary conditions indicate that (i) the probability of electron reflection from the rough sample edge is independent on the reflection angle φ and (ii) the transverse component of the electron flow,

$$j_y(y) = \frac{n_0}{\pi m} \int_0^{2\pi} d\varphi' \cos \varphi' f(y, \varphi'), \quad (\text{S6})$$

vanishes at the edges, $j_y|_{y=\pm W/2} = 0$, and, thus, everywhere in the sample due to the continuity equation $\text{div } \mathbf{j} = j' = 0$.

The longitudinal current density along the sample is defined as:

$$j_x(y) = \frac{n_0}{\pi m} \int_0^{2\pi} d\varphi' \sin \varphi' f(y, \varphi'). \quad (\text{S7})$$

If an electric current flows through a sample in a magnetic field, a perturbation of the charged density and the Hall electric field arise due to the magnetic Lorentz force. Both these effects are described by the zeroth ($m = 0$) angular harmonic of the distribution function:

$$f^{m=0}(y) = \frac{1}{2\pi} \int_0^{2\pi} d\varphi' f(y, \varphi'). \quad (\text{S8})$$

Figures S1(a,b) shows the regions in the (y, φ) -plane corresponding to the ballistic motion of electrons reflected from the right and the left sample edges. Here and below in the current work we imply that the electron mean free path $l = 1/\gamma$ is much longer than the sample width.

For narrow samples, $W \ll R_c$, the left and right ballistic regions are close to the rectangles $[-\pi/2, \pi/2] \times [-W/2, W/2]$ and $[\pi/2, 3\pi/2] \times$

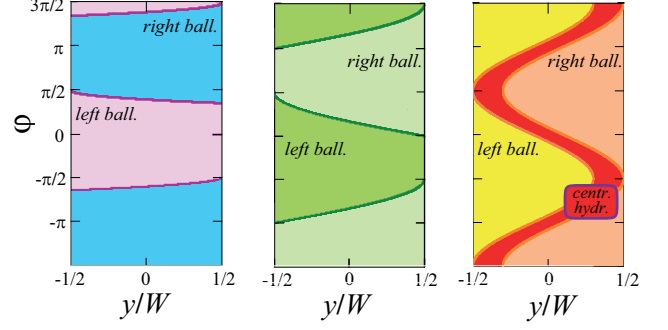


FIG. S1: Regions in the plane (y, φ) corresponding to the trajectories of the ballistic electrons, reflected from the left and the right sample edges (in all panels), as well as of the center hydrodynamic electrons, those do not scatter on the edges [red region in panel (c)]. The cases of narrow, $W \ll R_c$ (a); intermediate, $W \sim R_c$ (b); and wide, $W > 2R_c$ (c) are shown.

$[-W/2, W/2]$ [see Fig. S1(a)]. For wider samples, $W \sim R_c$, $W < 2R_c$, the boundaries of the left and right region $\varphi_{\pm}(y)$ begin to significantly depend on coordinate y [see Fig. S1(b)]. The very boundary curves $\varphi_{\pm}(y)$ coincide the electron trajectories those are touching the edges tangentially. Therefore the distribution function $f(y, \varphi)$ is not well defined at $\varphi = \varphi_{\pm}(y)$ and can have a discontinuity at these curves. At magnetic fields above the critical field, $W > 2R_c$, the central electrons those do not scatter on the edges arise in the region filled with red in Fig. S1(c). Herewith the edge electrons in the left and right regions (yellow and pink) still scatter mainly on the edges.

2. SOLUTION OF THE KINETIC EQUATION IN THE BALLISTIC REGIME

2.1. General solution

In this section we consider the 2D electron transport in a long sample in a weak magnetic field corresponding to the diameter of the cyclotron circle larger than the sample width, $2R_c > W$. Provided the mean free path is much longer than the sample width, $l = 1/\gamma \gg W$, the most frequent type of electron scattering is collisions with the sample edges, therefore the electron transport is ballistic.

In this case it is useful to rewrite the kinetic equation (S2) in the form:

$$\begin{aligned} \left[\cos \varphi \frac{\partial}{\partial y} + \gamma \right] \tilde{f} - \sin \varphi E_0 &= \\ = \gamma_{ee} \hat{P}[\tilde{f}] + \gamma_d \hat{P}_0[\tilde{f}] + \omega_c \frac{\partial \tilde{f}}{\partial \varphi}, \end{aligned} \quad (\text{S9})$$

where we have introduced the function:

$$\tilde{f}(y, \varphi) = f(y, \varphi) + \phi(y). \quad (\text{S10})$$

Here, ϕ is the electrostatic potential of the Hall electric field $E_H = -\phi'$. Indeed, it follows from Eq. (S2) that the Hall potential $\phi(y)$ plays the same role in the transport equation as it's progenitor, the zero harmonic of the distribution function $f^{m=0}(y)$ (S8) being proportional to the inhomogeneous density perturbations. Therefore it is reasonable to introduce the function $\tilde{f}(y, \varphi)$ (S10) in order to take into account $\phi(y)$ and $f^{m=0}(y)$ within the same framework.

The zero harmonic $\tilde{f}^{m=0}(y)$ of the generalized distribution function (S10) takes the form:

$$\tilde{f}^{m=0}(y) = \delta\mu(y) + \phi(y), \quad (\text{S11})$$

where $\delta\mu$ is the perturbation of the electron chemical potential. In the case of sufficiently slow flows, the values $\delta\mu(y)$ and $\phi(y)$ are related by the electrostatic relations [19]. For the considered case of 2D identical degenerate electrons, the electrostatic potential ϕ is usually much greater than the corresponding perturbation of the chemical potential $\delta\mu$ [19]. Thus the Hall electric field is calculated just by the formula $E_H(y) \approx -[\tilde{f}^{m=0}]'(y)$.

For brevity, we further omit the tilde in the function \tilde{f} and write $f \equiv \tilde{f}$.

In Ref. [25] we considered the kinetic equation (S9) in the limits $\gamma W \gg 1$ and $\gamma W \ll 1$ at zero magnetic field. First, we demonstrated that the hydrodynamic regime is realized in the limit $\gamma W \gg 1$ in the central region of the sample, $W/2 - |y| \gg 1/\gamma$. In this domain, both sides of Eq. (S9) are of the same order of magnitude and it is transformed into the Navier-Stokes equation for the density of the electron flow $j_x(y)$.

Second, we have shown Ref. [25] that in the ballistic regime, $\gamma W \ll 1$, the terms $\cos \varphi \partial f / \partial y$ and $\sin \varphi E_0$ in the left-hand side of Eq. (S9) are much larger than the arrival terms $\gamma_{ee} \hat{P}[f]$ and $\gamma_d \hat{P}_0[f]$ in the right-hand side in the factor of $\ln[1/(\gamma W)]$, therefore the last terms can be taking into account in the solution by the perturbation theory. Herewith the departure term γf in the left-hand side plays role of regularization of the kinetic equation near the angles $\varphi \approx \pi/2$, where the coefficient of the term $\cos \varphi \partial f / \partial y$ is close to zero.

In Ref. [26] we have obtained the similar result for equation (S9) at a nonzero magnetic field. Namely, in weak magnetic fields, $\omega_c \ll \gamma^2 W$, the terms $\gamma_{ee} \hat{P}[f]$ and $\gamma_d \hat{P}_0[f]$ should be treated as perturbations in the equations for the first, $f_1 \sim \omega_c$, and the second, $f_2 \sim \omega_c^2$, order corrections by magnetic field to the distribution function $\tilde{f}(y, \varphi)$, those are responsible for the Hall effect and the magnetoresistance in the ballistic regimes.

It is reasonable to expect that at intermediate magnetic field,

$$\omega_c \sim 1/W, \quad \omega_c < 2/W, \quad (\text{S12})$$

where the vanishing of the term $\cos \varphi \partial f / \partial y$ at $\varphi \approx \pi/2$ is "healed" by the magnetic field term $\omega_c \partial f / \partial \varphi$, only the collisions with the edges determine the electron flow. The neglect of the collision terms in kinetic equation (S9) leads to the following estimates

$$f \sim \frac{E_0}{\omega_c}, \quad j \sim j_0, \quad E_H \sim E_0, \quad (\text{S13})$$

where we have introduced the typical amplitude of the current density, $j_0 = n_0 E_0 W / m$. According to such estimate of f , both the arrival and the departure terms are proportional to $(\gamma / \omega_c) E_0 \ll E_0$ and thus are much smaller than the other terms of Eq. (S9). Consequently, in this regime the bulk collision terms in kinetic equation (S9) actually lead only to small corrections to the distribution function, being proportional to the small parameter γ / ω_c .

Below we will show that the above approximation (S13) is valid in the ballistic region, $\omega_c < 2/W$, except (i) the region of very weak fields, $\omega_c \ll \gamma^2 W$, studied in Refs. [25],[26], and (ii) in the vicinity of transition point, $0 < 2 - \omega_c W \lesssim \gamma W$, where the electron-electron collisions (and/or scattering on the bulk disorder) start to play crucial role.

In this way, we divide the ballistic regime on the three subregimes:

$$(i) \quad \omega_c \ll \gamma^2 W \quad (\text{S14})$$

{the case studied in Refs. [25, 26], in which the magnetic field provides only small correction to the flow};

$$(ii) \quad \gamma^2 W \ll \omega_c \ll 1/W \quad (\text{S15})$$

[the case when the magnetic field parameter $\omega_c W$ is small, and the bulk scattering provides only small corrections to the flow]; and

$$(iii) \quad \omega_c \sim 1/W, \quad 2 - \omega_c W \gg \gamma W \quad (\text{S16})$$

[the case when the magnetic field parameter $\omega_c W$ is of order of unity or close to the critical value, 2, and the bulk scattering still provides only small corrections].

According to the above discussed results of Refs. [25, 26] and estimations characterizing the cases (ii) and (iii), in order to develop a unified description of the ballistic transport in all the subregimes (i)-(iii) one should use the kinetic equation (S9) with only the departure collision term:

$$\left[\cos \varphi \frac{\partial}{\partial y} + \gamma \right] f - \sin \varphi e E_0 = \omega_c \frac{\partial f}{\partial \varphi}. \quad (\text{S17})$$

This equation can be solved by the method of characteristics. Apparently, this was done for the first time in recent publication [24]. In our work, using a slightly different approach, we obtain the ballistic solution $f(y, \varphi)$

similar to the one obtained in Ref. [24]. We use this solution to study the regimes those were not considered in Ref. [24]: the first ballistic subregime (i), $\omega_c W \ll \gamma^2 W^2$, and the singular part of the third subregion (iii), $\gamma W \ll 2 - \omega_c W \ll 1$. Moreover, for the second ballistic subregion (ii), $\gamma^2 W^2 \ll \omega_c W \ll 1$, we derive from $f(y, \varphi)$, analytical formulas for the current density $j(y)$ and the Hall electric field $E_H(y)$, those were not obtained in Ref. [24].

The solution of Eq. (S17) with boundary conditions (S4) and (S5) is a discontinuous function with the domains of continuity shown in Figs. S1(a,b). For the electrons reflected from the left edge, whose trajectories lie in the diapason:

$$\begin{aligned} -\pi + \arcsin[1 - \omega_c(W/2 - y)] < \varphi < \\ < \arcsin[1 - \omega_c(W/2 + y)], \end{aligned} \quad (\text{S18})$$

[see Fig. S1(a,b)] we introduce the following notation for the distribution function: $f(y, \varphi) = f_+(y, \varphi)$, while for the electrons reflected from the right edge, whose trajectories are located in the diapason

$$\begin{aligned} \arcsin[1 - \omega_c(W/2 + y)] < \varphi < \\ < \pi + \arcsin[1 - \omega_c(W/2 - y)], \end{aligned} \quad (\text{S19})$$

[see Fig. S1(a,b)] we introduce the analogous notation: $f(y, \varphi) = f_-(y, \varphi)$. The functions f_{\pm} are calculated by the method of characteristic for the first-order differential equation (S17). After some algebra, we obtain:

$$\begin{aligned} f_{\pm}(y, \varphi) = \frac{E_0}{\gamma^2 + \omega_c^2} \left[\omega_c \cos \varphi + \gamma \sin \varphi + \right. \\ \left. + e^{\gamma\varphi/\omega_c} Z_{\pm}(\sin \varphi + \omega_c y) \right], \end{aligned} \quad (\text{S20})$$

where the y -independent terms $\omega_c \cos \varphi$ and $\gamma \sin \varphi$ are particular solutions of Eq. (S17) those corresponds to the usual Drude formulas (provided γ is rate of electron scattering on disorder), while the term $e^{\gamma\varphi/\omega_c} Z_{\pm}(X)$ is a general solution of kinetic equation (S17) [without the field term $\sin \varphi E_0$], satisfying the proper boundary conditions (S4).

By substituting Eq. (S20) into boundary conditions (S4), we obtain the explicit form of $Z_{\pm}(X)$:

$$\begin{aligned} Z_+(X) = e^{-\gamma \arcsin(X + \omega_c W/2)/\omega_c} \left[c_l - \right. \\ \left. -\gamma(X + \omega_c W/2) - \omega_c \sqrt{1 - (X + \omega_c W/2)^2} \right] \end{aligned} \quad (\text{S21})$$

and

$$\begin{aligned} Z_-(X) = e^{-\gamma [\pi - \arcsin(X - \omega_c W/2)]/\omega_c} \left[c_r - \right. \\ \left. -\gamma(X - \omega_c W/2) - \omega_c \sqrt{1 - (X - \omega_c W/2)^2} \right], \end{aligned} \quad (\text{S22})$$

where the coefficients c_l and c_r are determined from balance relations (S5) of the boundary conditions. The resulting linear equations for c_l and c_r takes the form:

$$\begin{pmatrix} I_{ll} & I_{lr} \\ I_{rl} & I_{rr} \end{pmatrix} \begin{pmatrix} c_l \\ c_r \end{pmatrix} = - \begin{pmatrix} I_l \\ I_r \end{pmatrix}, \quad (\text{S23})$$

where the coefficients in the first line of the matrix are expressed via the integrals:

$$I_{ll} = 2 + \int_{-\pi + \varphi_0}^{-\pi/2} d\varphi \cos \varphi e^{\gamma(\pi + 2\varphi)/\omega_c} \quad (\text{S24})$$

and

$$I_{lr} = 2 + \int_{\pi/2}^{\pi + \varphi_0} d\varphi \cos \varphi \times \quad (\text{S25})$$

$$\times e^{\gamma [\varphi - \pi + \arcsin(\sin \varphi - \omega_c W)]/\omega_c},$$

while the first components of the right-hand vector is:

$$\begin{aligned} I_l = \frac{\pi \omega_c}{2} + \int_{\varphi_0}^{\pi/2} d\varphi \cos \varphi \times \\ \times e^{\gamma(2\varphi - \pi)/\omega_c} (\omega_c \cos \varphi - \gamma \sin \varphi) - \\ - \int_{-\pi/2}^{\varphi_0} d\varphi \cos \varphi e^{\gamma [\varphi - \arcsin(\sin \varphi + \omega_c W)]/\omega_c} \times \\ \times [\omega_c \sqrt{1 - (\sin \varphi + \omega_c W)^2} + \gamma (\sin \varphi + \omega_c W)]. \end{aligned} \quad (\text{S26})$$

The other coefficients in Eq. (S23), I_{rr} , I_{rl} and I_r , are related to I_{ll} , I_{lr} , and I_l by the formulas:

$$I_{rr} = -I_{ll}, \quad I_{rl} = -I_{lr}, \quad I_r = I_l. \quad (\text{S27})$$

In Eqs. (S24)-(S26) we introduced the notation: $\varphi_0 = \arcsin(1 - \omega_c W)$.

At general values of the parameter $\omega_c W$, integrals (S24)-(S27) can be calculated only numerically. However, the explicit expressions of the integrals and the values $c_{l,r}$ and $j(y)$, $E_H(y)$ can be obtained in the limiting cases: $\omega_c W \ll (\gamma W)^2$ [the first ballistic subregion (i)]; $(\gamma W)^2 \ll \omega_c W \ll 1$ [the second ballistic subregion (ii)]; and $0 < 2 - \omega_c W \ll 1$ [the right singular part of the third ballistic subregion (iii)].

2.2. Fully ballistic transport in moderately weak magnetic fields

Analysis of Eqs. (S20)-(S27) shows that in the intermediate magnetic fields, $\omega_c W \gg (\gamma W)^2$ and $2 - \omega_c W \gg \gamma W$

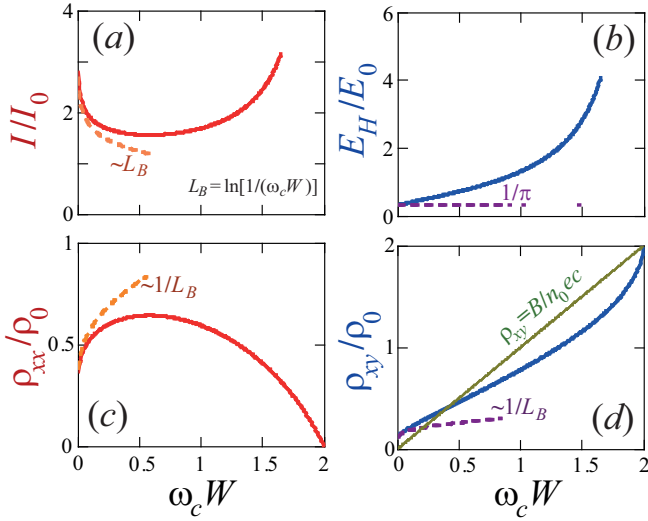


FIG. S2: Total current (a), Hall electric field (b), longitudinal (c) and Hall resistances (d) for the sample with no bulk scattering, $\gamma = 0$, as functions of magnetic field in the second, $0 < \omega_c W \ll 1$, and the third, $1 \lesssim \omega_c W < 2$, ballistic subregimes.

[the second and the third ballistic subregimes], the electron motion is determined predominantly by the ballistic effects: the scattering on the edges and the action of the fields E_0 and B . Herewith the bulk scattering (electron-electron collisions and/or the scattering on disorder) provides only small corrections to it.

So in order to describe the flow in the main order by the parameter γW in the above diapason of ω_c , we derive from Eq. (S20) the asymptote by $\gamma \rightarrow 0$:

$$f_{\pm}(y, \varphi) = \tilde{c}_{l,r} + \frac{E_0}{\omega_c} \left\{ \cos \varphi \mp \sqrt{1 - \left[\sin \varphi + \omega_c \left(y \pm \frac{W}{2} \right) \right]^2} \right\}, \quad (\text{S28})$$

where $\tilde{c}_{l,r} = E_0 c_{l,r} / \omega_c^2$. The solution of Eq. (S20) at $\gamma = 0$ can be determined up to a constant term, that corresponds to the fact that perturbations of the electron density do not relax. Imposing the symmetric condition $c_l + c_r = 0$, we find from system (S23):

$$\tilde{c}_{l,r} = \mp \frac{E_0}{\omega_c} \frac{U - V}{2(2 - \omega_c W)}, \quad (\text{S29})$$

where

$$U = \arccos(1 - \omega_c W), \quad (\text{S30})$$

$$V = (1 - \omega_c W) \sqrt{\omega_c W} \sqrt{2 - \omega_c W}.$$

We note that solution (S28) has already been obtained in recent work [24].

In Fig. S2 we show the numerically calculated dependencies of the total current:

$$I = \int_{-W/2}^{W/2} dy j_x(y), \quad (\text{S31})$$

the averaged Hall electric field:

$$E_H = \int_{-W/2}^{W/2} \frac{dy}{W} E_H(y), \quad (\text{S32})$$

and the resistances $\varrho_{xx} = E_0/I$, $\varrho_{xy} = E_H/I$ in the entire ballistic region $0 < \omega_c < 2/W$ for the fully ballistic sample with the absence of any bulk scattering, $\gamma = 0$. We see from Fig. S2 that the estimates (S13) for I and E_H are indeed valid in the middle part of the interval, where $\omega_c \sim 1/W$. The current $I(\omega_c)$ diverges at the both edges of this interval, while the Hall field $E_H(\omega_c)$ diverges only at $\omega_c W \rightarrow 2$ being finite at $\omega_c \rightarrow 0$. Such singular behavior of the flow in the limits $\omega_c W \rightarrow 0$ and $\omega_c W \rightarrow 2$ was not studied in Ref. [24].

The existence of a constant finite of the Hall field E_H in the limit of low fields, $\omega_c \rightarrow 0$, is an unusual fact associated with the ballistic character of the motion. The behavior of $\varrho_{xy}(B)$ of such type was previously obtained in numerical simulations [27] and was called the ballistic magnetoresistance anomalies. Namely, the dependence $\varrho_{xy}(B)$ in Fig. S2(d) and Fig. S5(d) is similar to “the last Hall plateau” arising in 2D electron transport in ballistic junctions [27]. In the next subsection, we will show from general solution (S20) that taking into account any bulk scattering leads to a linear fall of the Hall field E_H with magnetic field at $\omega_c \rightarrow 0$.

Near the transition point, $\gamma W \ll 2 - \omega_c W \ll 1$, the coefficients $\tilde{c}_{l,r}$ diverge rapidly:

$$\tilde{c}_{l,r} = \pm \frac{\pi E_0}{2\omega_c(2 - \omega_c W)}. \quad (\text{S33})$$

They becomes greater than the other terms in Eq. (S28) and, thus, represent the main part of the distribution function. Such distribution function means that, in order to compensate the part of the nonequilibrium flows $j_y|_{y=\pm W/2}$ induced by action of the fields E_0 and B on electron trajectories, there arises an imbalance between the densities of electrons reflected from the left and the right edges.

In the limit of small magnetic fields, $\omega_c W \ll 1$, the main contribution to the transport characteristics is given by electrons moving along the sample edges with angles $\varphi \approx \pm\pi/2$. The asymptotic form of the distribution function (S28) for the angles $\sqrt{\omega_c W} \ll |\pi/2 - \varphi| \ll 1$ is given by:

$$f_{\pm}(y, \varphi) = \tilde{c}_{l,r} + E_0 \left[(y \pm W/2) \frac{\sin \varphi}{\cos \varphi} + \omega_c \frac{(y \pm W/2)^2}{2} \left(\frac{1}{\cos \varphi} + \frac{\sin^2 \varphi}{\cos^3 \varphi} \right) \right], \quad (\text{S34})$$

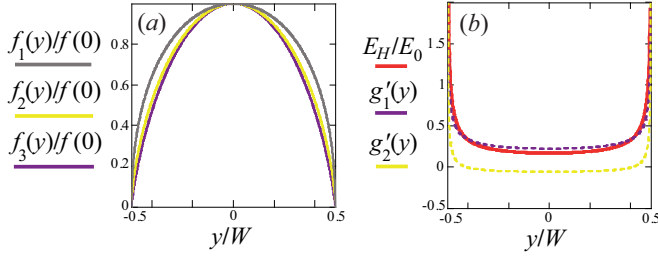


FIG. S3: Functions, which determine the profiles of the current density (a) and the Hall field (b) according to Eqs. (S36) and (S40) in the singular part of the second ballistic region, $(\gamma W)^2 \ll \omega_c W \ll 1$, when the interparticle scattering can be neglected. On the panel (a) all functions $f_1(y)$, $f_2(y)$, and $f_3(y)$ are normalized to their maximal values $f_1(0)$, $f_2(0)$, and $f_3(0)$. Red curve in panel (b) correspond to the total Hall field given by Eq. (S40).

where

$$\tilde{c}_{l,r} = \pm \frac{\sqrt{2}}{3} E_0 \sqrt{\omega_c W^3}. \quad (\text{S35})$$

The current density $j(y) \equiv j_x(y)$ at $\omega_c W \ll 1$ corresponding to Eq. (S34) consists of the main part, being independent on the coordinate y , and a small y -dependent correction by the logarithmic parameter $\ln[1/(\omega_c W)] \gg 1$:

$$j(y) = j_B + \Delta j(y),$$

$$\frac{j_B}{j_0} = \frac{1}{\pi} \ln\left(\frac{1}{\omega_c W}\right), \quad j_0 = \frac{n_0 E_0 W}{m}, \quad (\text{S36})$$

$$\frac{\Delta j(y)}{j_0} = f_1(y) + f_2(y) + f_3(y).$$

These formulas provide the main contribution j_B to the current by the parameter $\omega_c W$, being proportional to $\ln[1/(\omega_c W)]$, and the next-order y -dependent correction, which is of the order of unity. Functions $f_1(y)$, $f_2(y)$ and $f_3(y)$ are plotted in Fig. S3(a). They have rather similar profiles with infinite derivative at the sample edges $y = \pm W/2$

$$f_1(y) = \frac{1}{\pi} \left(\sqrt{\frac{1}{2} + \frac{y}{W}} + \sqrt{\frac{1}{2} - \frac{y}{W}} \right), \quad (\text{S37})$$

$$f_2(y) = \frac{1}{\pi} \left\{ \left(\frac{1}{2} + \frac{y}{W} \right) \ln \left[\frac{\sqrt{2}}{\sqrt{\frac{1}{2} + \frac{y}{W}}} \right] + \left(\frac{1}{2} - \frac{y}{W} \right) \ln \left[\frac{\sqrt{2}}{\sqrt{\frac{1}{2} - \frac{y}{W}}} \right] \right\}, \quad (\text{S38})$$

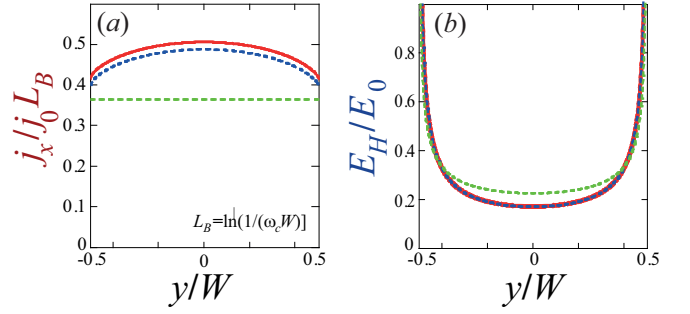


FIG. S4: Current density and Hall field in the second ballistic subregime at $\gamma = 0$ and $\omega_c W \ll 1$, namely $\omega_c W = 10^{-3}$. The results of the direct numerical calculations are colored in red. Blue curves are plotted by analytical formulas (S36) and (S40). Green curve in panel (a) correspond to the main contribution $j_B \sim L_B = \ln[1/(\omega_c W)] \gg 1$. The mismatch of the blue and red curves for the current density is due to higher order corrections in $1/L_B$, which are not taken into account in Eq. (S36). Green curve in panel (b) represents the contribution proportional to $g_1'(y)$ in Eq. (S40). It is the main contribution to $E_H(y)$ since $g_2'(y)$ is proportional to small numeric factor.

and

$$f_3(y) = \frac{1}{\pi} \left\{ \left(\frac{1}{2} + \frac{y}{W} \right) \ln \left[\frac{\sqrt{2}}{1 - \sqrt{\frac{1}{2} - \frac{y}{W}}} \right] + \left(\frac{1}{2} - \frac{y}{W} \right) \ln \left[\frac{\sqrt{2}}{1 - \sqrt{\frac{1}{2} + \frac{y}{W}}} \right] \right\}. \quad (\text{S39})$$

The expression for the potential of the Hall electric field potential has the similar form:

$$\phi(y) = E_0 W [g_1(y) + g_2(y)], \quad (\text{S40})$$

where

$$g_1(y) = \frac{1}{2\pi} \left(\sqrt{\frac{1}{2} + \frac{y}{W}} - \sqrt{\frac{1}{2} - \frac{y}{W}} \right) \quad (\text{S41})$$

and

$$g_2(y) = \frac{1}{2\pi} \left\{ \left(\frac{1}{2} + \frac{y}{W} \right) \ln \left[\frac{1 - \sqrt{\frac{1}{2} - \frac{y}{W}}}{\sqrt{\frac{1}{2} + \frac{y}{W}}} \right] + \left(\frac{1}{2} - \frac{y}{W} \right) \ln \left[\frac{1 - \sqrt{\frac{1}{2} + \frac{y}{W}}}{\sqrt{\frac{1}{2} - \frac{y}{W}}} \right] \right\}. \quad (\text{S42})$$

These formulas describe the Hall field in the main order by the parameter $\omega_c W \ll 1$. Both the functions $g_1(y)$ and $g_2(y)$ have the derivatives tending to infinity at the sample edges, thus the Hall electric field $E_H(y) = -\phi'(y)$ diverge at the edges [see Fig. S3(b)].

In Fig. S4 we compare the results of the numerical calculation of the profiles $j(y)$ and $E_H(y)$ based on the

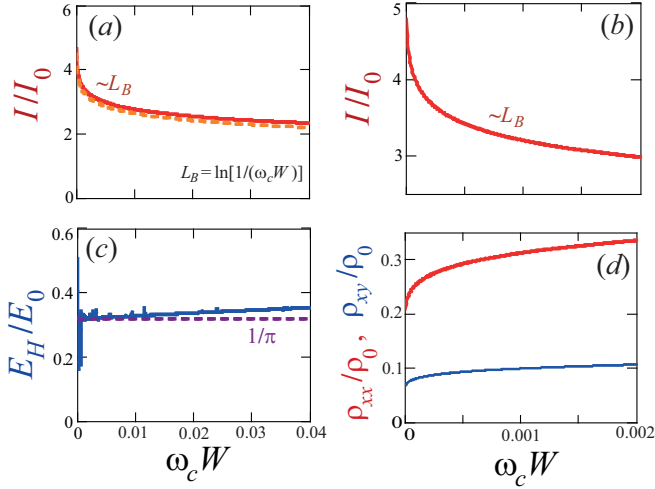


FIG. S5: Total current (a,b), Hall electric field (c), longitudinal and Hall resistances (d) at $\gamma = 0$ as functions of magnetic field in the second ballistic subregion, $0 < \omega_c W \ll 1$, where the distribution function is determined mainly by the ballistic trajectories of electrons and the parameter $\omega_c W$ is small. Solid lines represent the result of numerical calculations using (S28). Dashed lines are plotted after analytical results (S36) and (S40).

exact distribution function (S28) with analytical expressions (S36) and (S40). We see from the figure that the analytical curves (S36) and (S40) describe well the current and the Hall field in the limit $\omega_c W \ll 1$.

Figure S5 shows graphs of the total current, the averaged Hall field and the corresponding resistances in the second ballistic subregion, $\omega_c W \ll 1$. The current possesses a weak logarithmic singularity at low fields $I(\omega_c) \sim \ln[1/(\omega_c W)]$, while the Hall field exhibits the mentioned above anomalous behavior $E_H(\omega_c) \rightarrow \text{const}$ at $\omega_c \rightarrow 0$. Thereby the resistances ϱ_{xx} and ϱ_{xy} both exhibit similar singular behavior $\varrho_{xy} \sim 1/\ln[1/(\omega_c W)]$ and $\varrho_{xx} \sim 1/\ln[1/(\omega_c W)]$.

2.3. Transport in very weak magnetic fields

The general solution (S20) at a finite bulk scattering rate γ can be greatly simplified in the limit of very weak magnetic field, $\omega_c \ll \gamma^2 W$ (S14) [the first ballistic subregime (i)]. In this region, the effect from a magnetic field can be treated as a perturbation and the distribution function f_{\pm} (S20), including the values c_{\pm} , can be expanded in powers of the parameter $\omega_c W \rightarrow 0$. The continuity domains of $f_{\pm}(y, \varphi)$ given by (S18) and (S19) become independent of y and reduce to $-\pi/2 < \varphi < \pi/2$ and $\pi/2 < \varphi < 3\pi/2$ [see Fig. S1(a)]. Analysis shows that inequality (S14) allows to omit the contribution from the skipping electrons with $|\varphi| \approx \pi/2$ to all values.

In the zeroth order by ω_c , functions f_{\pm} (S20) take the

well-known form [27],[25]:

$$f_{\pm}(y, \varphi) = E_0 \frac{\sin \varphi}{\gamma} \left[1 - \exp \left(-\gamma \frac{y \pm W/2}{\cos \varphi} \right) \right], \quad (\text{S43})$$

with the zero coefficients $c_{l,r}$. The flow density corresponding to Eq. (S43) in the leading order by the parameter γW is homogeneous, while a y -dependence emerges in the next order by γW [25]:

$$\begin{aligned} j(y) &= j_{\gamma} + \Delta j(y), \\ \frac{j_{\gamma}}{j_0} &= \frac{2}{\pi} \ln \left(\frac{1}{\gamma W} \right), \quad j_0 = \frac{n_0 E_0 W}{m}, \\ \frac{\Delta j(y)}{j_0} &= -\frac{2}{\pi} \left[\left(\frac{1}{2} + \frac{y}{W} \right) \ln \left(\frac{1}{2} + \frac{y}{W} \right) + \right. \\ &\quad \left. + \left(\frac{1}{2} - \frac{y}{W} \right) \ln \left(\frac{1}{2} - \frac{y}{W} \right) \right]. \end{aligned} \quad (\text{S44})$$

The current $\Delta j(y)$ profile again has infinite derivatives at the sample edges $y = \pm W/2$ [see Fig. S6(a)].

As it follows from Eq. (S43), the logarithmic divergence in j_{γ} by γ originates from the electrons whose the velocity angles lie in the diapason: $||\varphi| - \pi/2| \lesssim \delta_m$, where $\delta_m = \gamma W \ll 1$. Such electrons move almost parallel to the sample edges and spend much longer time between scattering in the edges as compared with other electrons having the angles $\varphi \sim 1$. Therefore the first electrons acquire much larger velocity contributions due to acceleration by the electric field E_0 , $v_x(t) = E_0 t$.

In Refs. [25, 26] a solution of Eq. (S17) based on the perturbation theory by the magnetic field term was constructed. Up to the second order in ω_c , such distribution function has the form: $f = f_0 + f_1 + f_2$, where f_0 is function (S43), while $f_1 \sim \omega_c$ and $f_2 \sim \omega_c^2$. It was shown in Refs. [25, 26] that the applicability criterion of such power decomposition coincides with definition (S14) of the first ballistic subregime.

Direct calculations yield that, the function f_1 derived in Ref. [26] coincides with the first order term in the expansion of f_{\pm} (S20) in the powers of ω_c . This function satisfies the nontrivial boundary conditions (S4) with $c_{l,r} \neq 0$ and can be written as $f_1 = f_1^z + \delta f_1$, where

$$\begin{aligned} f_1^z(y, \varphi) &= \omega_c E_0 \left\{ \frac{\cos \varphi}{\gamma^2} - \exp \left[-\gamma \frac{y \pm W/2}{\cos \varphi} \right] \right. \\ &\quad \left. \times \left[\frac{\cos \varphi}{\gamma^2} + \frac{y \pm W/2}{\gamma} - \frac{\sin^2 \varphi}{2 \cos^3 \varphi} \left(y \pm \frac{W}{2} \right)^2 \right] \right\} \end{aligned} \quad (\text{S45})$$

is the solution of the inhomogeneous kinetic equation ($E_0 \neq 0$) with zero boundary conditions, while the term

$$\delta f_1(y, \varphi) = \mp \omega_c E_0 \frac{W}{4\gamma} \exp \left(-\gamma \frac{y \pm W/2}{\cos \varphi} \right), \quad (\text{S46})$$

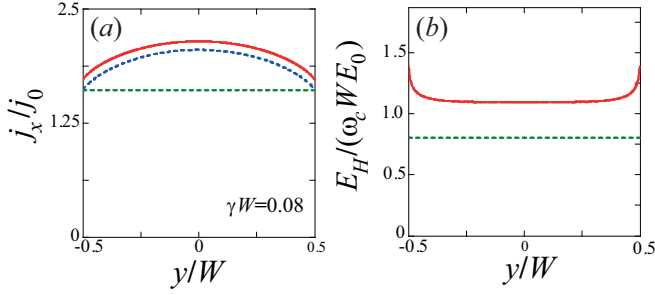


FIG. S6: Current density (a) and Hall field (b) in the first ballistic subregime corresponding to $\omega_c W \ll (\gamma W)^2$ at $\gamma W = 0.08$. Red curves present numerical results for $j(y)$ and $E_H(y)$ obtained from integration of the distribution functions (S43), (S45), and (S46). Blue curve in panel (a) correspond to analytical solution (S44), while green curve shows the main contribution to the current density $j = j_\gamma$. Green curve in panel (b) is plotted according to Eq. (S47).

being the solution of the kinetic equation with $E_0 = 0$, ensures that the boundary conditions are met. The function δf_1 is much smaller than f_1^z at $|\varphi - \pi/2| \lesssim \delta_m$, however δf_1 and f_1^z give comparable contributions to $j_y(y)$.

Combining of Eqs. (S45), (S46), and (S8), we obtain for the Hall field in the leading order by γW [26]:

$$E_H(y) \equiv E_0 \frac{\omega_c W}{\pi} \ln\left(\frac{1}{\gamma W}\right). \quad (\text{S47})$$

The numerically calculated exact profile $E_H(y)$ corresponding to Eqs. (S45) and (S46) differs from this analytical formula (S47) by the values of the order of unity at general y and by the divergent peculiarities at the sample edges $y \rightarrow \pm W/2$ [see Fig. S6(b)]. These peculiarities in the Hall field near sample edges are similar to the ones in the second ballistic subregime, $(\gamma W)^2 \ll \omega_c W \ll 1$, when electron-electron collisions become insignificant [see Fig. S4(b)]. It is noteworthy that the Hall field (S47) is linear by magnetic field, like it takes place in conventional bulk conductors.

Results (S36) and (S47) were derived from the kinetic equation (S17) in the ballistic regime taking into account only the departure term $-\gamma f$ in the inter-particle collision integral and the magnetic field term $\omega_c \partial f / \partial \varphi$. Such description implies that the particles that after an edge-scattering event reach the other edge without inter-particle collisions (at velocity angles $|\varphi - \pi/2| \gg \delta_m$) or undergo an inter-particle collision (at $|\varphi - \pi/2| \lesssim \delta_m$) somewhere in the bulk. Herewith the main contribution to the current and the Hall field comes from the electrons with the velocity angles $\delta_m \lesssim |\pi/2 - |\varphi|| \ll 1$. Analogously, the value of the Hall electric field is mainly determined by the requirement of the balance of the Lorentz force and the Hall field acting on the ballistic electrons with the angles $\delta_m \lesssim |\varphi - \pi/2| \ll 1$.

Based on this physical picture, we below derive equations (S36) and (S47) in an simple physically transparent

way, not employing the kinetic equation.

In the limit of very weak external fields, $\omega_c \rightarrow 0$ and $E_0 \rightarrow 0$, electron trajectories are almost straight:

$$v_x(t, \varphi) = v_F \sin \varphi + \frac{eE_0}{m} t, \quad (\text{S48})$$

$$v_y(t, \varphi) = v_F \cos \varphi + \omega_c \int_0^t dt' v_x(t'; \varphi),$$

where the time t is counted from the moment of last reflection of an electron from an edge and we again write in this section the Fermi velocity v_F explicitly for better understanding.

The mean current density j is calculated the Drude formula $j = n_0 t_0 E_0 / m$, where t_0 is the mean time of electron free motion. In the first ballistic regime, the value t_0 is obtained by the proper averaging of the times $t_\pm(y = \pm W/2, \varphi)$ of collisionless motion of individual electrons between the edges. Here the value $t_\pm(y, \varphi)$ corresponds to the electron trajectories between the edge $y = \mp W/2$ and the point y , unperturbed by external field and described by the first terms in Eqs. (S48):

$$t_\pm(y, \varphi) = \frac{W/2 \pm y}{v_F |\cos \varphi|}. \quad (\text{S49})$$

In order to find t_0 , one needs to integrate $t_\pm(y = \pm W/2, \varphi)$ by φ up to the limiting values of $\varphi = \varphi_m \approx \pm \pi/2$ at which $|\pi/2 - |\varphi||$ is equal to $\delta_m \sim \gamma W$. Such limits correspond to the ballistic trajectories with the maximum length equal to the mean free path relative to the bulk scattering, $l = 1/\gamma$. After the integration, we obtain $j = j_\gamma$ for the mean current density, where j_γ is defined in Eq. (S44).

Next, we calculate the Hall field E_H within similar approach. We suppose that it is approximately homogeneous in y : $E_H(y) \approx E_H$. In order to find E_H , we use the y component of Newton's equations having the form:

$$m \dot{v}_y = e E_H + \frac{eB}{c} v_x. \quad (\text{S50})$$

After the averaging of this equating by φ , only the contribution to v_x related to the acceleration by the field E_0 [see Eq. (S48)] remains non-zero at any y . This fact and Eq. (S50) leads to the following estimate $\dot{v}_y, E_H \sim E_0 B$ in the limit $E_0, B \rightarrow 0$. Next, due to the sample edges, there is no acceleration along the y direction of the whole ensemble of electrons in the sample,

$$\int d\varphi \int dy m \dot{v}_y(t_\pm(y, \varphi), \varphi) = 0. \quad (\text{S51})$$

Equation (S50) averaged over all electrons in the samples [that is, integrated by $d\varphi/(2\pi)$ and dy/W with the same restriction on φ , $|\varphi - \pi/2| \lesssim \gamma W$] and condition (S51) yield result (S47) for the Hall electric field E_H .

Equations (S36) and (S47) lead to the following expression for the Hall resistance $\varrho_{xy} = E_H/j_\gamma$:

$$\varrho_{xy} = \frac{1}{2}\varrho_{xy}^0, \quad \varrho_{xy}^0 = \frac{m\omega_c}{n_0} = \frac{B}{n_0ec}, \quad (\text{S52})$$

where ϱ_{xy}^0 is the conventional Hall resistance for the Ohmic and the hydrodynamic flows of charged particles at low temperatures. Owing to the above elementary calculation procedure, it becomes apparent that the factor 1/2 in Eq. (S52) has a kinematic origin. It is related to the need to compensate the Hall field for the linearly increasing in time acceleration of runaway electrons.

The second-order correction $f_2 \sim \omega_c^2$ to the electron distribution function was also calculated in Ref. [25]. At the velocity directions being close to the sample direction, $|\varphi - \pi/2| \ll 1$, the function f_2 in the main order by $1/(\gamma W)$ has the form:

$$\begin{aligned} f_2(y, \varphi) &= \frac{\omega_c^2 E}{2 \cos^5 \varphi} \left(y \pm \frac{W}{2}\right)^3 \times \\ &\times \left[1 - \frac{1}{4} \left(y \pm \frac{W}{2}\right) \frac{\gamma}{\cos \varphi}\right] \times \\ &\times \exp \left[-\frac{\gamma}{\cos \varphi} \left(y \pm \frac{W}{2}\right)\right]. \end{aligned} \quad (\text{S53})$$

This correction leads to a magnetic field dependence of the current density:

$$j = j_\gamma + j_2, \quad j_2 = \frac{3n_0 E_0}{2\pi m} \frac{\omega_c^2}{W\gamma^4}. \quad (\text{S54})$$

We see from this formula that the magnetic field magnitude corresponding to the inequality $j_2 \ll j_\gamma$ is given by the inequality $\omega_c \ll \gamma^2 W \ln^{1/2}[1/(\gamma W)]$, which is similar, up the logarithm $\ln[1/(\gamma W)]$, to definition (S14) of the first ballistic subregion. The origin of correction (S55) consists in a small increase of the mean length of the electron collisionless trajectories between the sample edges at nonzero magnetic fields (see Fig. 1 in Ref. [25]).

The obtained positive correction to the current, j_2 (S54), leads to the small negative magnetoresistance:

$$\frac{\varrho_{xx}(B) - \varrho_{xx}(0)}{\varrho_{xx}(0)} = -\frac{3\omega_c^2}{4\gamma^4 W^2 \ln[1/(\gamma W)]}, \quad (\text{S55})$$

where $\varrho_{xx}(0) = E_0/j_\gamma$. It was discussed in Refs. [25, 26] that for not too long samples, $W \ll L \ll 1/\gamma$, the bulk scattering rate γ in this formula is replaced on the reciprocal sample length, $1/L$, and the magnetoresistance (S55) becomes temperature-independent.

3. MEAN FIELD SOLUTION IN A VICINITY OF THE PHASE TRANSITION

3.1. Ballistic solution near the critical field

For simplicity, we consider only two types of samples in which only one of the scattering mechanisms acts: the electron-electron collisions ($\gamma_d = 0$, $\gamma = \gamma_{ee}$) or the scattering on disorder ($\gamma_{ee} = 0$, $\gamma = \gamma_d$).

In this subsection, from general ballistic solution (S20), we obtain the simplified distribution function in the low vicinity, $0 \ll 2 - \omega_c W \ll 1$, of the critical magnetic field $\omega_c^{cr} = 2/W$, taking into account the departure term $-\gamma f$ of the bulk scattering in the kinetic equation. Such distribution function is a generalization of the fully ballistic solution (S33), that neglects any bulk scattering and is valid only in the part of the vicinity of ω_c^{cr} : $\gamma W \ll 2 - \omega_c W \ll 1$. The solution of this subsection provides a proper description of the transport at $\omega_c W < 2$ in the disordered samples and is a block of the theory of the transport at $\omega_c W < 2$ in pure sample with electron-electron collisions.

The coefficients I_{ll} , I_{lr} of the system of linear equations (S23) tend to zero at $2 - \omega_c W \ll 1$. From Eqs. (S24) and (S25) for I_{ll} , I_{lr} in main order by the small parameters $2 - \omega_c W \ll 1$ and $\gamma/\omega_c \ll 1$ we have:

$$I_{ll} = 2 - \omega_c W + \frac{2\pi\gamma}{\omega_c}, \quad I_{lr} = 2 - \omega_c W. \quad (\text{S56})$$

Herewith, it follows from Eq. (S26) that the right-hand side coefficients in Eq. (S23) remains finite:

$$I_l = -\pi\omega. \quad (\text{S57})$$

From Eqs. (S23), (S56), and (S57) we obtain that the parameters c_\pm in distribution function (S20) takes the form:

$$c_\pm = \pm \frac{\omega_c/2}{\gamma/\omega_c + (2 - \omega_c W)/\pi}, \quad (\text{S58})$$

We see that such c_\pm demonstrate a divergent behavior at $\omega_c \rightarrow \omega_c^{cr}$, becoming much larger than unity. In this regard, the main contribution to the distribution function (S20) is:

$$f_\pm(y, \varphi) = \frac{E_0}{\omega_c^2} c_\pm. \quad (\text{S59})$$

The function f_\pm (S59) describes a redistribution of electrons between the left and the right regions (S18) and (S19) [see Fig. S1], being homogeneous in each region. At $2 - W/R_c \ll 1$, the most of inequilibrium electrons described by f_\pm (S59) are the skipping electrons, those after the reflection from an edge returns to the same edge. Only a very small fraction of reflected electrons reaches the opposite edge [see Fig. S1 and Fig. 1(b) in the main

text]. The $\mathbf{E} \times \mathbf{B}$ -drift flow in the y direction, described by the space-homogeneous Drude part of the distribution function (S20), is compensated by the electrons reaching the opposite edge, as each skipping electron provide no contribution to the flow in the y direction. The density of the inequilibrium electrons reaching the opposite edge is proportional to the coefficients c_{\pm} times the small relative part of such electrons. This explains why the coefficients c_{\pm} at $\omega_c W \rightarrow 2$ must be very large.

Beside this, there is a small part of the skipping electrons, which would have returned to the same edge, but, due to an electron-electron collision, will not actually return. Such electrons leads to an additional compensation of the $\mathbf{E} \times \mathbf{B}$ drift flow and, thus, weakens the imbalance between the electrons in the left and right regions. That is why the divergence of c_{\pm} at $\omega_c W \rightarrow 2$ is limited by the scattering rate γ [see Eq. (S58)].

The current density and the Hall electric field for distribution function (S59) in the main order by γ and ε takes the forms:

$$j(y) = \frac{2nE_0}{\pi m} \frac{1}{\gamma + \varepsilon} \sqrt{1 - \omega_c^2 y^2}, \quad (\text{S60})$$

and

$$E_H(y) = \frac{E_0}{\pi} \frac{1}{\gamma + \varepsilon} \frac{\omega_c}{\sqrt{1 - \omega_c^2 y^2}}. \quad (\text{S61})$$

where the parameter ε characterizing the proximity to the transition point:

$$\varepsilon = \frac{2 - \omega_c W}{\pi} \omega_c \quad (\text{S62})$$

These profiles correspond to the following averaged values of the current density $j = \int_{-W/2}^{W/2} dy j(y)/W$ and the mean Hall field $E_H = \int_{-W/2}^{W/2} dy E_H(y)/W$:

$$j = \frac{n_0 E_0}{m} \frac{1}{2(\gamma + \varepsilon)} \quad (\text{S63})$$

and

$$E_H = E_0 \frac{\omega_c}{2(\gamma + \varepsilon)}. \quad (\text{S64})$$

Functions (S60) and (S61) as well as the profiles $j(y)$ and $E_H(y)$ in the other ballistic subregimes are plotted in Fig. S7.

It is of importance to perform a more precise calculation of the current density j and the Hall electric field E_H for the critical distribution function (S59). We obtain in the next order by the small parameter $\sqrt{\varepsilon}$ the same equation (S63) for the mean current density and the formula:

$$E_H = E_0 \frac{\omega_c}{2(\gamma + \varepsilon)} F(\varepsilon), \quad F(\varepsilon) = 1 - \sqrt{2\varepsilon/\pi}, \quad (\text{S65})$$

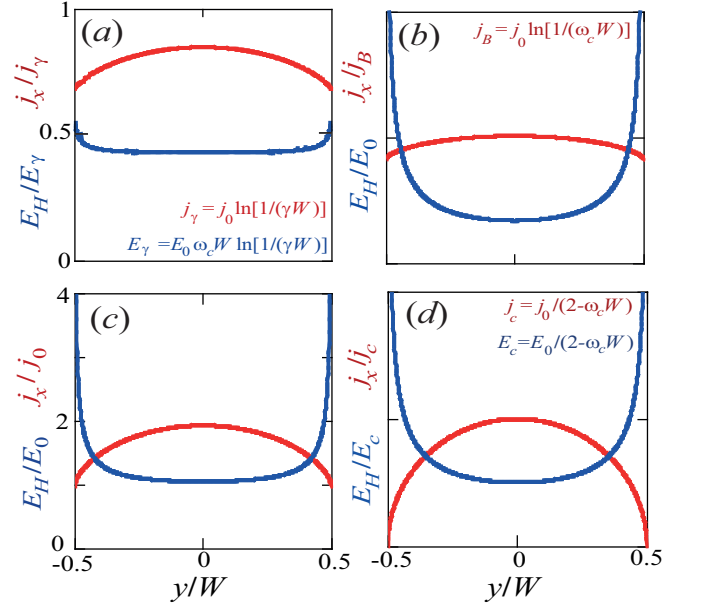


FIG. S7: Profiles of the current density (red curves) and the Hall electric field (blue curves) for different values of magnetic field, corresponding to: (a) the first ballistic subregime, $\omega_c \ll \gamma^2 W$, for the zero-field ballistic parameter $\gamma W = 0.08$; (b) the second ballistic subregime, corresponding to the small parameter $\omega_c W$, $\omega_c W = 10^{-3}$ [herewith $\omega_c W \gg (\gamma W)^2$]; (c) the third ballistic subregime at the intermediate parameter $\omega_c W$, $\omega_c W = 1$; and (d) the very point of the phase transition, when $\omega_c W = 2$. Curves are plotted by formulas (S7) and (S8) with the distribution functions (S43), (S45), (S46) for panel (a); (S28) for panels (b) and (c); and (S59) for panel (d).

for the Hall field. The factor $F(\varepsilon)$ describes the correction to Eq. (S64) related to deviations of the shapes of the left and the right ballistic regions from their limiting form at $\varepsilon = 0$ (see Fig. S1). So equations (S63) and (S65) describe the current and the Hall field near the transition within the mean field approximation in the two first orders by the parameter $\sqrt{\varepsilon}$ and in the main order by the parameter γ .

For brevity, below we omit the factor n_0/m in all current densities.

It is noteworthy that the obtained values of the ballistic current (S63) and the Hall field (S64) at the transition point $\omega_c W = 2$ turn out to be one half as compared with those obtained within the Drude model for a bulk sample of the same width with the rate γ of the scattering on disorder. Thus, for disordered samples with no interparticle collisions the scattering on the rough edges and the scattering on the bulk disorder provide the same additive contributions to the total momentum relaxation rate 2γ , appearing in current (S63) and Hall field (S64).

3.2. Mean field theory below the critical field

In the case of interacting electrons in the absence of disorder, in the nearest vicinity of the critical magnetic field,

$$0 < 2 - \omega_c W \lesssim \gamma / \omega_c, \quad (\text{S66})$$

substitution of the singular distribution function f_{\pm} (S59) into the departure and the arrival terms, γf and $\gamma \hat{P}[f]$, leads to the values of the same order of magnitude as the external field term, $\sim E_0 \sin \varphi$. This indicates that both the terms γf and $\gamma \hat{P}[f]$ are equally important in the region near the transition.

Our approach to the description of the dynamic in interval (S66) is based on taking into account the arrival term $\gamma \hat{P}[f]$ in the way analogous to the mean field theory for thermodynamic phase transitions. In our approach, we treat the part of the term $\gamma \hat{P}[f]$ proportional to $\sin \varphi$:

$$\gamma \hat{P}_{\sin}[f](y, \varphi) = \gamma j(y) \sin \varphi, \quad (\text{S67})$$

as an addition “internal” electric field [see Eqs. (S7) and (S9)]. Herewith we omit its dependence on the coordinate y replacing the factor $j(y)$ in Eq. (S67) by its average value $j = \int_{-W/2}^{W/2} dy j(y) / W$.

It was shown in Ref. [26] that, in the first ballistic subregime, $\omega_c \ll \gamma^2 / W$, where $j(y)$ is close to j_{γ} [see Eq. (S44)], this approach is exact in the main order by the large logarithmic parameter $\ln[1/(\gamma W)]$ and allows one to calculate small corrections to the current and the Hall field from the the arrival term $\gamma \hat{P}[f]$. Near the transition, the ballistic current density $j(y)$ (S60) is strongly inhomogeneous and, thus, such approach is not exact [see Eq. (S60)]. However, in accordance with the practice of applying the mean field approximation in thermodynamic phase transition, it is reasonable to believe that such mean field approach will provide a qualitatively correct description of the phase transition.

Let us note that replacing of the arrival term $\gamma \hat{P}[f]$ by its value average by y can be interpreted as using of a special, nonlocal by y , collision integral:

$$\text{St}'[f](y, \varphi) = -\gamma \left\{ f(y, \varphi) - \int_{-W/2}^{W/2} \frac{d\xi}{W} \hat{P}[f](\xi, \varphi) \right\}. \quad (\text{S68})$$

Such collision integral conserves momentum and number of electrons only within the whole sample, but not at a given point y . In this regard, the solution of the kinetic equation with Eq. (S68) leads to a non-physical current $j_y(y)$ and a density perturbation, $\delta n(y)$, proportional to the small parameter γW .

In this way, the self-consistent mean field equation for description of the behavior of the order parameter $j = j(\varepsilon)$, depending on magnetic field via ε , is constructed by

the substitution:

$$E_0 \rightarrow E_0 + \gamma j \quad (\text{S69})$$

in equation (S63). After it, we obtain the self-consistent equation for the current in the right (singular) part of the third ballistic subregion (S66):

$$j = \frac{E_0 + \gamma j}{2(\gamma + \varepsilon)}. \quad (\text{S70})$$

Solution of this equation yields:

$$j = \frac{E_0}{\gamma + 2\varepsilon}. \quad (\text{S71})$$

In the very transition point, $\varepsilon = 0$, this value is twice as large compared with the fully ballistic result (S63), that neglects the arrival term in the kinetic equation.

Result (S71) implies the following electron dynamics.

For magnetic fields close to the critical one, electron-electron collisions not only lead to the departure of electrons from the ballistic trajectories along which they would return to the same edge, but also to the arrival of electrons from the skipping trajectories near the opposite edge. Due to the opposite signs of the coefficients c_{\pm} in the ballistic distribution function (S59), there is a drawback of the skipping electrons near the opposite edge. So the corresponding “negative arrival” of electrons from the opposite edge due to the arrival term provides the same contribution to the compensation of the $\mathbf{E} \times \mathbf{B}$ -drift along the y direction as compared with the “positive departure” due to the departure term. As a result, current (S71) at the very ballistic-hydrodynamic transition turns out to be twice as large as the ballistic current (S63), not taking into account the “negative arrival” described by renormalization (S69).

The Hall electric field with taking into account the arrival term is calculated by the same replacement $E_0 \rightarrow E_0 + \gamma j$ in equation (S65) for the ballistic Hall field taking into account only the departure term. We emphasize that equation (S65), unlike Eqs. (S63) and (S70), does not participate in the self-consistent procedure of determining the state of the system. Using mean field current (S71), we obtain from Eqs. (S65) and (S69):

$$E_H = (E_0 + \gamma j) \frac{\omega_c}{2(\gamma + \varepsilon)} F(\varepsilon), \quad (\text{S72})$$

that leads to:

$$E_H = E_0 \frac{\omega_c}{\gamma + 2\varepsilon} F(\varepsilon). \quad (\text{S73})$$

Due to the factor $F(\varepsilon)$, this function has a strong square-root singularity at $\omega_c W \rightarrow 2$.

3.3. Mean field theory above the critical field

In samples wider than the twice cyclotron radius, there arises a group of the electrons whose trajectories do not

cross the sample edges [see Fig. S1(c) and Fig. 1(c) in the main text]. Such “center” electrons spend a long time, $\sim 1/\gamma \gg W$ on their trajectories without collisions. It is reasonable to expect that the appearance the center electrons dramatically changes the transport regime. Their relative density,

$$\alpha_c = (W - 2R_c)/W = 1 - 2/\omega_c, \quad (\text{S74})$$

can be considered as the order parameter of the ballistic-hydrodynamic and the ballistic-Ohmic phase transitions. The fraction of the other “edge” electrons those are scattered mainly on the edges is equal to:

$$\alpha_e = 2R_c/W = 1 - \alpha_c. \quad (\text{S75})$$

As we will see below, the center electrons are a nucleus of the hydrodynamic or the Ohmic flow when the electron-electron scattering or the scattering on disorder dominates, respectively.

In order to find the distribution functions f_e and f_c of the edge electrons (“e”) and of the central electrons (“c”), one should distinguish the regions in the (y, φ) plane where the central electrons or the edge electrons are located [see Fig. S1(c)] and solve kinetic equation (S9) with both the arrival and the departure terms. As the electron-electron bulk scattering is much less intensive than the collisions of the edge electrons with the edges, the dynamic of the edge electrons is substantially different from the one of the center electrons. This is expressed by domination of the terms $\omega_c \partial f_e / \partial \varphi$ and $\partial f_e / \partial y$ on the departure, $-\gamma f_e$, as well as on the arrival scattering term, $\gamma P[f_e + f_c]$, (or $\gamma P_0[f_e + f_c]$ for the disordered case). Note that only the last term mixes the functions f_e and f_c .

Instead of an exact solution of the kinetic equation, we propose a two-component mean field model accounting both the groups of electrons. Our model is qualitatively applicable, as we believe, in the upper vicinity of the phase transition:

$$0 < \omega_c W - 2 \ll 1, \quad (\text{S76})$$

It is based on using of the mean field ballistic solution [Eqs. (S71) and (S72)] for the edge electrons and the Drude-type formulas for the small fraction of the center electrons (see below).

In order to describe the center electrons, it is convenient to change the variables y, φ on the new variables y_c, φ , where y_c is the coordinate of the center of electron cyclotron orbits. The positions of the central electrons are characterized by the inequality:

$$-W/2 + R_c < y_c < W/2 - R_c, \quad (\text{S77})$$

and their velocity angle φ takes any values. For the edge electrons we have:

$$|y_c| > W/2 - R_c, \quad (\text{S78})$$

and their velocity angle φ lies in the diapason depending on y_c . Using of the ballistic mean field results (S71) and (S72) for the contribution from the center electrons implies that the exact domains of definition of the function f_e as well as the detailed properties of f_e and f_c are not important for calculation of total j and E_H .

First, we study the ballistic-hydrodynamic transition in pure samples when only the electron-electron scattering takes place.

If the fraction of the central electrons is small, $\alpha_c \ll 1$, the centers of their cyclotron orbits lies approximately in the center of the sample, $y = 0$ [see Eq. (S77) and Fig. 1(c) in the main text]. Due to their low density, $\alpha_c \ll 1$, the central electrons most often scatter on the edge electrons. At different y_c , described by Eq. (S77) at $W/2 - R_c \ll W$, the central electrons are scattered on the edge electrons with the same distribution $f_e(y_c, \varphi)$, which varies significantly on the scale of the order W . Thus the properties of the central electrons in the main order by γ and α_c are described by the distribution function f_c substantially depending on φ and being weakly dependent on y :

$$f_c(y_c, \varphi) \approx f_c(0, \varphi). \quad (\text{S79})$$

Thus for the description of the state of the central electrons, the use of only one mean field parameter, for example, the effective current density j_c related to f_c (S79), is a good approximation. Herewith, for the description of the state of the edge electrons we use the mean field parameter j_e , introduced in the previous subsection. Indeed, ballistic kinetic equation (S17) with the arrival term simplified according to (S69) and boundary conditions (S4) is still applicable in the main order by $\gamma \ll \omega_c$ and $\alpha_c \ll 1$ for the left and the right edge electrons. Thus in the main order by the parameter γ , solution f_{\pm} (S59) at $\varepsilon = 0$ with effective field E_0 (S69) remains valid also for the edge electrons.

In this way, the mean field approach above the critical field $\omega_c = \omega_c^{cr}$ consists in taking into account the arrival terms with the functions f_e and f_c by the substitution:

$$E_0 \rightarrow E_0 + \gamma(j_e + j_c) \quad (\text{S80})$$

in ballistic functions f_{\pm} (S59).

Integration of function (S59) of the edge electrons with the factor $\sin \varphi$ over the left and the right regions (see Fig. S1) yields in the main order by α_c and γ the same result as integration of f_{\pm} (S59) at smaller (critical) magnetic field $\omega_c = 2/W$ over the whole sample. Thus the edge electron contributions is given by Eq. (S70) with the factor α_e :

$$j_e = \alpha_e \frac{E_0 + \gamma(j_e + j_c)}{2\gamma}. \quad (\text{S81})$$

In order to calculate the contribution from the central electrons in the current, we multiply the kinetic equation

(S9) expressed in the variables φ, y_c on the factor $\sin \varphi$ and integrate it by φ and y_c over $-\pi/2 < \varphi < 3\pi/2$ and $-W/2 + R_c < y_c < W/2 - R_c$. In this diapason the distribution function describes the central electrons and is given by Ref. (S79). As the result, we arrive to the formula:

$$j_c = \alpha_c \frac{E_0 + \gamma(j_e + j_c)}{\gamma}. \quad (\text{S82})$$

This is actually the Drude formula for the contribution to the total current from central electrons in the effective field (S80), which are scattered on the edge electrons with the rate γ .

Solving together the resulting system of mean field equations (S81) and (S82) and keeping in mind that $\alpha_e + \alpha_c = 1$, we obtain in the main order by γ :

$$j_e = \frac{E_0}{\gamma}, \quad j_c = 2\alpha_c \frac{E_0}{\gamma}. \quad (\text{S83})$$

The physical picture implied under the second equation is as follows. The dynamics of the central electrons in the reference frame moving with the drift velocity of the edge electrons, $\sim E_0/\gamma$, is similar to the scattering on static defects (that is the edge electrons look like static defects in the moving frame). The effective momentum relaxation time of the edge electrons is equal to $1/\gamma$ [see Eq. (S83)]. The time of the electron-electron scattering of the central electrons on the edge electrons is also $1/\gamma$. As the actual mean velocity of the central electrons is the sum of and their mean velocity in the moving frame and the mean velocity of the edge electrons, a doubling of the scattering time $1/\gamma$ in equation (S83) arises.

For the total current we obtain from Eq. (S83):

$$j = (1 + 2\alpha_c) \frac{E_0}{\gamma}. \quad (\text{S84})$$

According to the definition of α_c , this function grows linearly with the difference $B - B_c$ [see Fig. S7(a)].

The Hall electric field above the transition also contains the contributions from the edge electrons and from the center ones. As the ballistic solution f_{\pm} (S59) with the effective field (S80) remains approximately valid for the edge electrons at $0 < \omega_c W - 2 \ll 1$, the Hall field in the main order by γ is given by equation (S72). In it, we should put $\varepsilon = 0$ and use Eq. (S84) for the current j , and introduce the factor α_e accounting the relative density of the edge electrons. We obtain:

$$E_{H,e} = \alpha_e (1 + \alpha_c) \frac{\omega_c}{\gamma} E_0, \quad (\text{S85})$$

that is equal to $\omega_c E_0/\gamma$ in the main order by α_c .

The contribution to the Hall field from the central electrons is defined by the distribution function $f_c(y_c, \varphi) \approx f_c(0, \varphi)$. Multiplying kinetic equation (S9) on $\cos \varphi$ and integrating over $-\pi/2 < \varphi < 3\pi/2$ and $-W/2 + R_c <$

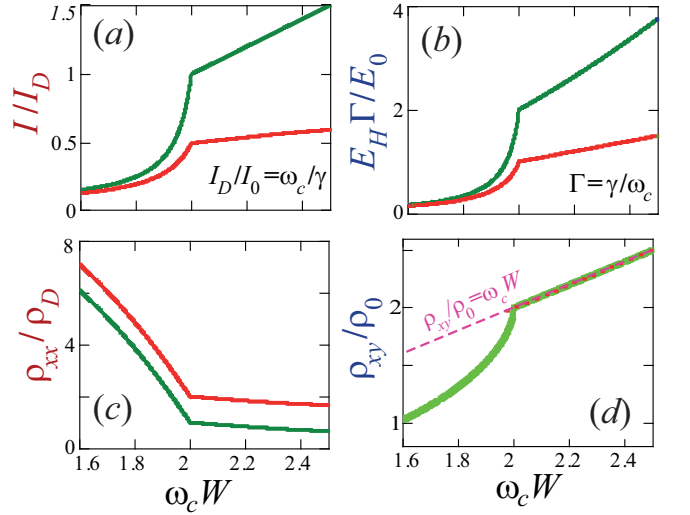


FIG. S8: Current (a), Hall electric field (b), longitudinal (c) and Hall (d) resistances as functions of magnetic field in a wide region around the critical field, $\omega_c W = 2$, for the ballistic-hydrodynamic phase transition [green curves] and for the ballistic-Ohmic phase transition [red curves]. In panel (d) for the Hall resistances the green and red curves corresponding to the both types of the transitions coincide.

$y_c < W/2 - R_c$, we obtain the contribution to the Hall field, similar to the result in the Drude theory:

$$E_{H,c} = \omega_c j_c. \quad (\text{S86})$$

From Eq. (S83) we get that the averaged Hall field consisting of the contributions (S85) and (S86) takes the form:

$$E_H = (1 + 2\alpha_c) \frac{\omega_c}{\gamma} E_0. \quad (\text{S87})$$

Second, let us consider the ballistic-Ohmic phase transition in a sample where only scattering on disorder is substantial.

In such system the dynamics of the groups of the edge and the central electrons are independent. For the contributions to j and E_H from edge electrons one should use just the pure ballistic formulas (S63) and (S64) at $\varepsilon = 0$, multiplied on the fraction of the edge electrons α_e :

$$j_e = \alpha_e \frac{E_0}{2\gamma}, \quad E_{H,e} = \alpha_e \frac{\omega_c}{2\gamma} E_0. \quad (\text{S88})$$

For the contribution to the current and the Hall field from the central electrons scattering on disorder we should use the Drude formulas with the factor α_c accounting their relative density:

$$j_c = \alpha_c \frac{E_0}{\gamma}, \quad E_{H,c} = \alpha_c \frac{\omega_c E_0}{\gamma}. \quad (\text{S89})$$

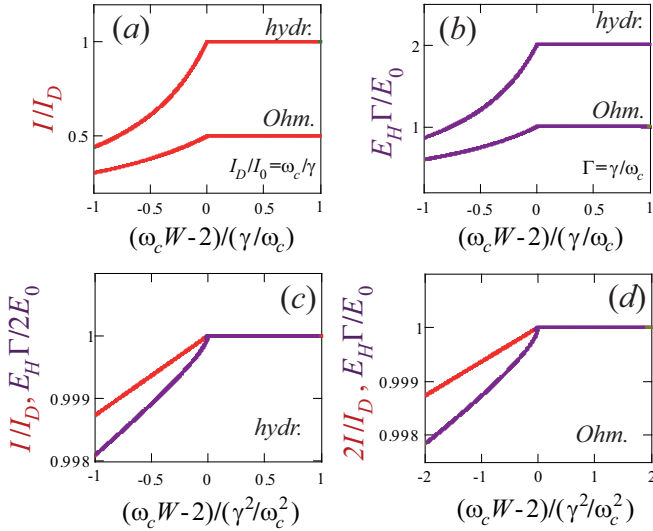


FIG. S9: Current (red lines) and Hall electric field (purple lines) as functions of magnetic field in a narrow (a,b) and in a very narrow (c,d) vicinities of the critical point $\omega_c W = 2$ for the ballistic-hydrodynamic and for the ballistic-Ohmic phase transition (see the captions on curves and on panels).

Keeping in mind that $\alpha_c + \alpha_e = 1$, for the mean current density and the Hall field we obtain:

$$j = \frac{1 + \alpha_c}{2} \frac{E_0}{\gamma}, \quad E_H = \frac{1 + \alpha_c}{2} \frac{\omega_c E_0}{\gamma}. \quad (\text{S90})$$

Unlike the samples where only the electron-electron scattering takes place in the bulk, in the disordered samples results (S90) remains valid at any relation between the fractions α_c and α_e of electrons of the both groups. In particular, in the limit of very large fields, when $W \gg R_c$ and $\alpha_c \approx 1$, equations (S90) turn into the usual Drude formulas for a long disordered sample.

From the obtained results we see that, in both the ballistic-hydrodynamic and the ballistic-Ohmic phase transitions, the dependence of the current on magnetic field, $j(\omega_c)$, has a jump of its derivative (a kink) at the critical field $\omega_c^{cr} = 2/W$, while the Hall field $E_H(\omega_c)$ has even a square root singularity at ω_c^{cr} (see Figs. S8 and S9).

Of particular interest is the behavior of the Hall resistance $\varrho_{xy} = E_H/j$ [see Fig. S8(d)]. The dependence $\varrho_{xy}(\omega_c)$ for both the ballistic-hydrodynamic and ballistic-Ohmic transitions coincide one with another. Above the transitions ϱ_{xy} is identically equal to its “standard” value $\varrho_{xy}^0 = B/n_0 e c$, corresponding to the Ohmic regime at low temperatures.

On the contrary, the behavior of the current and the corresponding longitudinal resistance near the transition field are quite different for the two phase transitions (see Fig. S10).

Finally, let us briefly discuss the behavior of the central electron far beyond the transition, when $W - 2R_c \sim W$

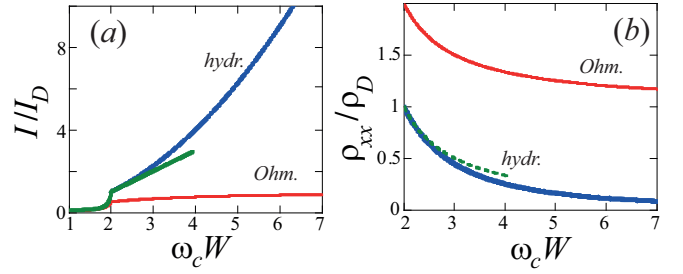


FIG. S10: Current (a) and longitudinal resistance (b) as functions of magnetic field near [schematic] and far beyond [Eqs. (S91) and (S92)] the critical field $\omega_c = 2/W$ for the ballistic-hydrodynamic and the ballistic-Ohmic phase transitions. Green curves correspond to the calculation for the vicinity of the ballistic-hydrodynamic phase transition by formulas (S84), which do not take into account the inhomogeneous distribution of central electrons.

and $\alpha_c, \alpha_e \sim 1$. In this regime, the collisions between the central electrons becomes important. The central electrons located farther from the edges are less likely to collide with edge electrons than central electrons located closer to the edge. This leads to the beginning of the formation of an inhomogeneous profile of the Poiseuille flow.

In the limit $W \gg R_c$ for the longitudinal resistance in disordered samples we obtain from Ref. (S90) the Drude resistance, being independent on ω_c :

$$\varrho_D(\omega_c) = \gamma, \quad (\text{S91})$$

i.e., the conventional formula $m\gamma/(n_0 e^2)$ in usual units.

In hydrodynamic samples, at magnetic fields, $\omega_c \gtrsim 1/W$, the central electrons begin to scatter predominantly on each other, and therefore the Poiseuille flow with a parabolic by y profile is formed. Such flow at large magnetic fields, $\omega_c \gg 1/W$, leads to the averaged resistance $\varrho_P = 12m\eta_{xx}/(ne^2 W^2)$ [15], where η_{xx} is the diagonal viscosity coefficient, being equal in our notations to $\eta_{xx} = \gamma/(16\omega_c^2)$ at $\gamma \ll \omega_c$. Thus, we obtain for the averaged sample resistance at $W \gg 1/\omega_c$ in our units:

$$\varrho_P(\omega_c) = \frac{3}{4} \frac{\gamma}{\omega_c^2 W^2}. \quad (\text{S92})$$

In this formula the contribution from the edge electrons is neglected. It is noteworthy that both resistances (S91) and (S92) are proportional to the scattering rate γ , but the second one decreases with the magnetic field as $\sim 1/(\omega_c W)^2$.

In Fig. S10 we schematically plot the dependencies $I(\omega_c)$ and $\varrho_{xx}(\omega_c)$ near and far above the transition ballistic-hydrodynamic and the ballistic-Ohmic transitions. At $0 < \omega_c W - 2 \ll 1$ these curves are described by Eqs. (S84) and (S87). At $\omega_c \gg 1/W$ they follow asymptotes (S91) and (S92). The region $\omega_c W - 2 \sim 1$ for the ballistic-hydrodynamic phase transition was studied by the numeric solution of the kinetic equation in Refs. [23],[24].

4. COMPARISON WITH PRECEDING THEORETICAL AND EXPERIMENTAL WORKS

4.1. Related theoretical works

In Ref. [23] a numerical solution of the kinetic equation (S2) is carried out for a similar system as we study in this work: a long narrow sample with rough edges. The kink in the dependencies of the resistances ϱ_{xx} and ϱ_{xy} on magnetic field B at the transition point $B = B_c$ was also obtained in Ref. [23]. Although the authors of Ref. [23] discussed the emergence of the central electrons above the transition those do not scatter on the edges, the electron dynamics just below the transition point $B = B_c$ and the interaction between the edge and the central electrons above $B = B_c$ were not considered.

The dependencies $\varrho_{xx}(B)$ and $\varrho_{xy}(B)$ presented in this work are very similar to the ones obtained in Ref. [23] for the narrow samples, $W \ll 1/\gamma$, with the exception of the region of the very small fields, $\omega_c \lesssim \gamma^2 W$ (the first ballistic subregime). In numerical calculation [23] this subregime was not pointed out, probably, because of a very slow convergence of the integrals by φ for the values j and E_H , which diverge logarithmically at $\gamma W \rightarrow 0$ [see Eqs. (S44) and (S47)].

In Ref. [24] the ballistic transport of 2D electrons in a long stripe was theoretically examined in details. Similar general formulas for the distribution function in the ballistic regime [see Eq. (S20)] and for the simplified distribution function in the second ballistic subregime [see Eq. (S28)] as well as the numeric description of the transport regime at $\omega_c W - 2 \sim 1$ were obtained. In the present paper we further develop the electron ballistic and hydrodynamic transport as compared with the results of Ref. [24]. Namely, in the current work we developed the qualitative description of the first and the third ballistic subregimes; derived the analytical expressions for $j(y)$ and $E_H(y)$ in all the three ballistic subregimes; and explained the origin of the Hall resistance $\varrho_{xy} = \varrho_{xy}^0/2$ in the limit $B \rightarrow 0$, and reveal the ballistic-hydrodynamic and the ballistic-Ohmic phase transitions.

4.2. Related experiments

As for the experimental observation of the ballistic-hydrodynamic phase transition and other predicted effects, we believe that they could be typically observed in high-quality and sufficiently narrow samples ($W \ll 1/\gamma$), where the ballistic transport regime is realized at $B = 0$. According to the developed theory, the transport in such systems becomes hydrodynamic (or Ohmic) with the increase of magnetic field B at $\omega_c > \omega_c^{cr} = 2/W$.

Below we briefly discuss experiments [6] and [13], in which, apparently, the smeared ballistic-hydrodynamic transition was already observed.

In Ref. [6] the Poiseuille flow of a 2D electron fluid in a graphene stripe was experimentally studied. Magnetoresistance and the distribution of the Hall field over the cross section of the stripe were measured in a wide range of magnetic fields and electron densities. The experimental dependence $\varrho_{xx}(B)$ is very similar to the theoretical one on Fig. 3(a) in the main text. It exhibits a nonmonotonous behavior at $B < B_c$, a smeared kink at the transition field $B = B_c$, and a monotonous decrease at $B > B_c$. However, a small peak in the vicinity of $B = 0$ related to the first ballistic subregime was not observed in the experimental data of Ref. [6]. This absence can be caused by the electron-electron scattering mean free path being larger than the sample length L {see Fig. 1(d) in Ref. [6]}. Thus, the ballistic dynamics studied in our work is apparently realized in the magnetic fields larger than some boundary field B_L corresponding to the equality $\sqrt{R_c W} = L$ and lying in the second ballistic subregime.

In Ref. [6] the Hall field profiles $E_H(y)$ were measured in the central part of the stripe. In the ballistic regime these profiles turned out to be nearly flat, while in the hydrodynamic regimes they were strongly curved (similar to the parabolic hydrodynamic profiles corresponding to the Poiseuille flow). We believe that the sharp features in $E_y(y)$ near the sample edges, $y = \pm W/2$, predicted by our theory for the ballistic regime [see Fig. S7 and Fig. 2 in the main text] can be observed in experiments similar to one of Ref. [6], provided the profiles $E_H(y)$ will be measured up to the sample edges.

In Ref. [14] authors observed the Poiseuille flow formed by 2D electrons in a long sample of high-mobility GaAs quantum wells. The dependence of the resistances ϱ_{xx} and ϱ_{xy} on magnetic field B were measured. Apparently, the system studied in Ref. [14] was close to the ballistic transport regime at $W < 2R_c$ and to the hydrodynamic regime at $W > 2R_c$. The experimental dependence $\varrho_{xx}(B)$ is rather similar to the theoretical one in Fig. 3(a) in the main text, with the exception of the small peak at very weak B . The experimental dependence $\varrho_{xy}(B)$ is also rather similar to the theoretical one obtained in the current work [see Fig. 3(b) in the main text]. Such dependence exhibits positive and negative deviations from the standard Hall resistance $\varrho_{xy}^0 = B/(nec)$ below the transition point, $W < 2R_c$, and an almost exact coincidence with ϱ_{xy}^0 above the transition point, $W > 2R_c$.

So the most of our theoretical prediction was observed in Refs. [6] and [13] with the exception of a negative temperature-independent magnetoresistance corresponding to the first ballistic subregime [the small peak at $B \rightarrow 0$, see Fig. 3(b) in the main text]. As it was discussed above, this feature is very sensitive to the sample geometry and its observability depends on the particular shape of the actual conductive channel in the sample.

As it was discussed in Refs. [25, 26], a negative

temperature-independent magnetoresistance corresponding to the small peak at $B \rightarrow 0$ related to the ballistic transport [see Fig. 3(b) in the main text] were apparently observed in high-mobility GaAs quantum wells containing macroscopic oval defects in Refs. [8–10]. Analysis [15] of the experimental results on the GaAs quantum wells analogous to the ones studied in Refs. [8–10] demonstrates that the effective width W_{eff} of the conductive

channel is apparently reduced due to the oval defects up to the mean distance between them. Therefore, it is reasonable to think that in the samples studied in Refs. [8–10] the ballistic regime was realized when the mean free path l was larger than the effective channel width W_{eff} and herewith the negative magnetoresistance corresponding to the first ballistic subregime was apparently observed in some samples.